

# Prospects for observing $2D$ and $1F$ charmonium states near 4 GeV

Zhi-Hao Pan<sup>1,2,3,4,6,\*</sup>, Cheng-Xi Liu<sup>1,2,3,4,6,†</sup>, Zi-Long Man<sup>1,2,3,4,6,‡</sup>, and Xiang Liu<sup>1,2,3,4,5,6,§</sup>

<sup>1</sup>*School of Physical Science and Technology, Lanzhou University, Lanzhou 730000, China*

<sup>2</sup>*Lanzhou Center for Theoretical Physics, Key Laboratory of Theoretical Physics of Gansu Province, Key Laboratory of Quantum Theory and Applications of MoE,*

*Gansu Provincial Research Center for Basic Disciplines of Quantum Physics, Lanzhou University, Lanzhou 730000, China*

<sup>3</sup>*MoE Frontiers Science Center for Rare Isotopes, Lanzhou University, Lanzhou 730000, China*

<sup>4</sup>*Research Center for Hadron and CSR Physics, Lanzhou University and Institute of Modern Physics of CAS, Lanzhou 730000, China*

Our understanding of high-lying states within the charmonium family remains incomplete, particularly in light of recent observations of charmonium states at energies around 4 GeV. In this study, we investigate the spectroscopic properties of several high-lying charmonia, focusing on the  $2D$  and  $1F$  states. A mass spectrum analysis is conducted, incorporating the unquenched effects. We then present a detailed study of the strong decay properties, including partial decay widths for two-body strong decays permitted by the Okubo-Zweig-Iizuka (OZI) rule. Additionally, we explore the primary radiative decay channels associated with these states. Finally, we discuss the productions of the  $2D$  and  $1F$  states via  $B$ -meson decay and  $e^+e^-$  annihilation. Theoretical predictions provided here aim to guide future experimental searches for high-lying charmonium states, particularly at BESIII, Belle II, LHCb and future facility STCF.

## I. INTRODUCTION

Since the 1974 discovery of the  $J/\psi$  particle [1, 2], numerous charmonium states have been experimentally observed, including the  $\psi(3686)$  [3],  $\eta_c(1S)$  [4],  $\eta_c(2S)$  [5],  $\psi(4040)$  [6],  $\psi(4415)$  [7],  $h_c(1P)$  [8],  $\chi_{c0}(1P)$  [9],  $\chi_{c1}(1P)$  [10],  $\chi_{c2}(1P)$  [11], and  $\psi(3770)$  [12]. These low-lying charmonium states have significantly influenced the development of theoretical models, particularly the Cornell potential model [13, 14], which provided a quantitative framework for hadron spectroscopy. Building on the Cornell model, several other potential models have been proposed [15–28], including the well-known Godfrey-Isgur (GI) model [24]. Collectively, these developments are generally classified under the category of quenched potential models.

Entering the 21st century, the discovery of new hadronic states, including the XYZ charmonium-like states [29–35], has significantly advanced hadron spectroscopy. This field serves as an essential tool for deepening our understanding of the non-perturbative behavior of the strong interaction. Among these discoveries, the observation of the  $X(3872)$  [36] garnered considerable attention and sparked widespread discussion within the whole community. The mass discrepancy between the  $X(3872)$  and the charmonium state  $\chi_{c1}(2P)$ , as predicted by the quenched potential model, led several research groups [37, 38] to propose the  $X(3872)$  as a  $D\bar{D}^*$  molecular state, while others argued for a tetraquark interpretation [39, 40]. The significance of unquenched effects [41–43] in hadron spectroscopy became increasingly recognized with the subsequent observation of the  $D_{s0}^*(2317)$  and  $D_{s1}(2460)$  mesons, following the discovery of the  $X(3872)$ . In this context, the  $X(3872)$  can still be classified as part of the charmonium family, as shown by studies employing the unquenched

potential model [44–48]. These developments underscore the importance of considering unquenched effects when studying hadron spectroscopy.

More recently, experiments have identified additional states, such as the  $\psi_3(3842)$  [49],  $\eta_c(3945)$ ,  $h_c(4000)$ ,  $\chi_{c1}(4010)$ , and  $h_c(4300)$  [50], along with heavier  $Y$  states, including  $Y(4544)$  [51],  $Y(4710)$  [52], and  $Y(4790)$  [53]. These discoveries show the possibility of constructing the charmonium family with high-lying states, offering a promising avenue to enhance our understanding of the hadron spectroscopy.

In fact, our understanding of high-lying charmonia remains limited compared to the well-established low-lying charmonia. Given the current state of knowledge, there is both strong motivation and significant interest in exploring the spectroscopic properties of high-lying states within the charmonium family. In this work, we focus on the  $2D$  and  $1F$  states. The mass spectrum and decay properties of these states are critical for their identification in future experiments. Therefore, it is essential to conduct a quantitative calculation to better understand these states.

To obtain the mass spectrum of the high-lying charmonia discussed here, we perform a mass spectrum analysis using a potential model that incorporates the unquenched effect. The mass spectrum of high-lying charmonia is also calculated in Refs. [46, 58–64] using various models. It is important to highlight the modified Godfrey-Isgur (MGI) model adopted in this work, an effective and successful unquenched approach for the quantitative analysis of high-lying hadron mass spectra [56, 65–70]. A key feature of the MGI model is its incorporation of the screened potential, which effectively reflects the unquenched effects and has proven successful in calculating the mass spectra of high-lying states [56, 69]. This modification is particularly important for accurately capturing the masses of higher radial and orbital excitations. In this study, we calculate the masses of high-lying states, including the ground states and the first and second radial excitations, for the  $D$ -,  $F$ -, and  $G$ -wave states. This allows us to construct a comprehensive charmonium family, extending from the  $S$ -

\* 220220939771@lzu.edu.cn

† liuchx2023@lzu.edu.cn

‡ manzl@lzu.edu.cn

§ xiangliu@lzu.edu.cn

$6^1S_0$	$6^3S_1$	$6^1P_1$	$6^3P_0$ $\chi_{c0}(4700)$ 4694 $^{+16}_{-10}$	$6^3P_1$ $\chi_{c1}(4685)$ 4684 $\pm 15$ 130 $\pm 40$	$6^3P_2$	$6^3D_1$	<div><div>Quantum number <math>(n^{2S+1}L_J)</math></div><div>State Mass (MeV) Width (MeV)</div></div>												<div><div></div>Candidate states</div>		<div><div></div>Established states</div>		<div><div></div>Our focused states</div>		<div><div></div>Missing states</div>											
$5^1S_0$	$5^3S_1$ $\psi(4415)$ 4415 $\pm 5$ 110 $\pm 22$	$5^1P_1$	$5^3P_0$ $\chi_{c0}(4500)$ 4474 $\pm 4$ 77 $\pm 10$	$5^3P_1$	$5^3P_2$	$5^3D_1$ $\psi(4660)$ 4641 $\pm 10$ 73 $\pm 11$																														
$4^1S_0$	$4^3S_1$ $\psi(4230)$ 4222 $\pm 2.3$ 49 $\pm 7$	$4^1P_1$	$4^3P_0$	$4^3P_1$ $\chi_{c1}(4274)$ 4286 $\pm 8.0$ 51 $\pm 7$	$4^3P_2$	$4^3D_1$ $\psi(4500)$ 4469 $\pm 26$ 246 $\pm 36$																														
$3^1S_0$	$3^3S_1$ $\psi(4040)$ 4040 $\pm 4$ 84 $\pm 12$	$3^1P_1$	$3^3P_0$	$3^3P_1$ $\chi_{c1}(4140)$ 4146 $\pm 3.0$ 19 $^{+10}_{-12}$	$3^3P_2$	$3^3D_1$ $\psi(4360)$ 4374 $\pm 7$ 118 $\pm 12$													$3^3D_2$	$3^3D_3$	$3^1D_2$	$3^1F_3$	$3^3F_2$	$3^3F_3$	$3^3F_4$	$3^1G_4$	$3^3G_3$	$3^3G_4$	$3^3G_5$							
$2^1S_0$ $\eta_{c(2S)}$ 3637 $\pm 0.9$ 11.8 $\pm 1.6$	$2^3S_1$ $\psi(2S)$ 3686 $\pm 0.011$ 0.293 $\pm 0.009$	$2^1P_1$	$2^3P_0$ $\chi_{c0}(3915)$ 3922 $\pm 0.18$ 20 $\pm 4$	$2^3P_1$ $\chi_{c1}(3872)$ 3871 $\pm 0.06$ 1.19 $\pm 0.21$	$2^3P_2$ $\chi_{c2}(3930)$ 3922 $\pm 1.0$ 35.2 $\pm 2.2$	$2^3D_1$ $\psi(4160)$ 4191 $\pm 5$ 69 $\pm 10$	$2^3D_2$	$2^3D_3$	$2^1D_2$	$2^1F_3$	$2^3F_2$	$2^3F_3$	$2^3F_4$	$2^1G_4$	$2^3G_3$	$2^3G_4$	$2^3G_5$																			
$1^1S_0$ $\eta_c$ 2984 $\pm 0.4$ 30.5 $\pm 0.5$	$1^3S_1$ $J/\psi$ 3096 $\pm 0.006$ 0.093 $\pm 0.002$	$1^1P_1$ $h_{c(1P)}$ 3525 $\pm 0.14$ 0.78 $\pm 0.28$	$1^3P_0$ $\chi_{c0(1P)}$ 3414 $\pm 0.3$ 10.7 $\pm 0.6$	$1^3P_1$ $\chi_{c1(1P)}$ 3510 $\pm 0.05$ 0.84 $\pm 0.04$	$1^3P_2$ $\chi_{c2(1P)}$ 3556 $\pm 0.07$ 1.98 $\pm 0.09$	$1^3D_1$ $\psi(3770)$ 3773 $\pm 0.7$ 27.2 $\pm 1.0$	$1^3D_2$ $\psi_2(3823)$ 3823 $\pm 0.34$ <2.9	$1^3D_3$ $\psi_3(3842)$ 3842 $\pm 0.2$ 2.8 $\pm 0.6$	$1^1D_2$	$1^1F_3$	$1^3F_2$	$1^3F_3$	$1^3F_4$	$1^1G_4$	$1^3G_3$	$1^3G_4$	$1^3G_5$																			
0 $^{--}$	1 $^{--}$	1 $^{+-}$	0 $^{++}$	1 $^{++}$	2 $^{++}$	1 $^{--}$	2 $^{--}$	3 $^{--}$	2 $^{+-}$	3 $^{+-}$	2 $^{++}$	3 $^{++}$	4 $^{++}$	4 $^{+-}$	3 $^{--}$	4 $^{--}$	5 $^{--}$																			

Quantum number ( $n^{2S+1}L_J$ )
State
Mass (MeV)
Width (MeV)

	Candidate states
	Established states
	Our focused states
	Missing states

FIG. 1: Table of Charmonium States. The yellow and green background colors represent well-established low-lying charmonium states [54] and high-lying charmonium states under investigation in this work, respectively. Significant progress has been made over the past few decades in constructing the charmonium family [30, 31, 34, 35, 55]. We have compiled the corresponding charmonium candidates[35, 56, 57], which are highlighted with a red background. In fact, charmonium is not limited to the states listed here; there are many more highly radial and orbital excited states.

wave to the  $G$ -wave.

After analyzing the mass spectrum of high-lying charmonium, we examine their two-body Okubo-Zweig-Iizuka (OZI)-allowed decays using the quark pair creation (QPC) model [71–74], a widely used model for calculating strong decays. By employing the MGI model, we derive the numerical wave functions for these charmonia, which are then used to calculate their strong decays. This allows us to obtain the partial and total decay widths, providing valuable insights for the identification of these states in future experiments. In addition to studying the strong decays of high-lying charmonia, we also investigate the electromagnetic transitions of charmonium. Radiative decays offer a crucial reference for identifying charmonium states in experiments. In conclusion, from a qualitative perspective, we have explored the potential production mechanisms of the  $2D$  and  $1F$  states to provide experimental references.

This paper is organized as follows. In Sec. II, we illustrate the MGI model and analyze the mass spectrum of charmonium states with MGI model. And then, in Sec. III we further study the corresponding two body OZI-allowed strong decay behaviors of the discussed states and compare our results with previous results [46]. Then, the calculation method of the radiative decays of singly charmonium states, along with the numerical results are given in Sec. IV. Finally, we summarize

and explore how the  $2D$  and  $1F$  may be observed.

## II. MASS SPECTRUM

In this study, we employ the MGI model to calculate the mass spectrum of the  $2D$ ,  $1F$ , and other high-lying charmonia. To obtain the mass spectrum, we introduce a screening potential within the MGI framework [56, 65–70]. The relevant Hamiltonian is

$$\tilde{H} = (p^2 + m_1^2)^{1/2} + (p^2 + m_2^2)^{1/2} + \tilde{V}_{\text{eff}}(\mathbf{p}, \mathbf{r}), \quad (1)$$

where  $m_1$  and  $m_2$  are equal and represent the mass of the  $c$  or  $\bar{c}$  quark, respectively. The effective potential  $\tilde{V}_{\text{eff}}(\mathbf{p}, \mathbf{r})$  describes the interaction between  $c$  and  $\bar{c}$ , including both a short-range one-gluon-exchange term  $\gamma^\mu \otimes \gamma_\mu$  and a long-range confinement term  $1 \otimes 1$ . In the non-relativistic limit,  $\tilde{V}_{\text{eff}}(\mathbf{p}, \mathbf{r})$  is reduced to the nonrelativistic potential  $V_{\text{eff}}(r)$ :

$$V_{\text{eff}}(r) = H^{\text{conf}} + H^{\text{hyp}} + H^{\text{so}}, \quad (2)$$

where

$$H^{\text{conf}} = br - \frac{4\alpha_s(r)}{3r} + c \quad (3)$$

is the spin-independent potential, which includes the confining potential, the Coulomb-like potential, and a constant term. Here,  $\alpha_s(r)$  is the running coupling constant. To account for the unquenched effect, it is common to replace the line potential with the screening potential:

$$br \rightarrow \frac{b(1 - e^{-\mu r})}{\mu}, \quad (4)$$

where  $\mu$  represents the strength of the screening effects. Therefore, the spin-independent potential in the MGI model becomes

$$H^{\text{scr}} = \frac{b(1 - e^{-\mu r})}{\mu} - \frac{4\alpha_s(r)}{3r} + c. \quad (5)$$

In our study, we employed the color-screening confinement potential model, constructed in 1995 [75]. This model demonstrates that the linear potential may be screened at large distances due to the creation of a light quark pair. Its formulation is inspired by earlier work in Lattice QCD [76]. With the growing number of observed hadronic states [54], this model has been applied to calculate hadron spectroscopy, including both light-flavor and heavy-flavor meson systems [56, 65, 66, 69, 77, 78], offering an effective approach to account for the unquenching effects. The importance of the unquenched effect was highlighted by the discovery of states like  $X(3872)$ ,  $D_{s0}(2317)$ ,  $D_{s1}(2460)$ , and  $\Lambda_c(2940)$ , which helped resolve the low-mass puzzle. These observations underscore that the study of hadron spectroscopy is entering a high-precision era, where unquenching effects cannot be overlooked. Currently, there are two primary methods for addressing the unquenched effect in hadron spectroscopy. One is the color-screening confinement potential model mentioned above, while the other involves coupled-channel analysis, which considers the coupling of bare states to allowed hadronic channels. As demonstrated in Refs. [57, 78], these two approaches are generally equivalent, with the color-screening confinement potential model effectively capturing the key features of the unquenched effect.

The color-hyperfine interaction  $H^{\text{hyp}}$  in Eq. (2) consists of the spin-spin and tensor terms, given by

$$H^{\text{hyp}} = \frac{4\alpha_s(r)}{3m_1m_2} \left[ \frac{8\pi}{3} \mathbf{S}_1 \cdot \mathbf{S}_2 \delta^3(\mathbf{r}) + \frac{1}{r^3} \left( \frac{3\mathbf{S}_1 \cdot \mathbf{r} \mathbf{S}_2 \cdot \mathbf{r}}{r^2} - \mathbf{S}_1 \cdot \mathbf{S}_2 \right) \right], \quad (6)$$

where  $\mathbf{S}_{1(2)}$  denotes the spin of the quark (antiquark). The spin-orbit interaction in Eq. (2) is expressed as

$$H^{\text{so}} = H^{\text{so(cm)}} + H^{\text{so(tp)}}. \quad (7)$$

Here,  $H^{\text{so(cm)}}$  represents the color-magnetic term, which can be written as

$$H^{\text{so(cm)}} = \frac{4\alpha_s(r)}{3r^3} \left( \frac{\mathbf{S}_1}{m_1^2} + \frac{\mathbf{S}_2}{m_2^2} + \frac{\mathbf{S}_1 + \mathbf{S}_2}{m_1m_2} \right) \cdot \mathbf{L}, \quad (8)$$

where  $\mathbf{L}$  is the relative orbital angular momentum between quark and antiquark.  $H^{\text{so(tp)}}$  is the Thomas precession term, with the screening effects expressed as

$$H^{\text{so(tp)}} = -\frac{1}{2r} \frac{\partial H^{\text{scr}}}{\partial r} \left( \frac{\mathbf{S}_1}{m_1^2} + \frac{\mathbf{S}_2}{m_2^2} \right) \cdot \mathbf{L}. \quad (9)$$

Additionally, the smearing transformation and momentum-dependent factors play a dominant role in the relativistic effects within the MGI model. On the one hand, we apply the smearing to the screened potential  $S(r) = \frac{b(1-e^{-\mu r})}{\mu} + c$  and the Coulomb-like potential  $G(r) = -\frac{4\alpha_s(r)}{3r}$ . For simplicity, we use the general symbol  $V(r)$  to represent both  $G(r)$  and  $S(r)$ . The smearing transformation is given by

$$\tilde{V}(r) = \int d^3\mathbf{r}' \rho(\mathbf{r} - \mathbf{r}') V(r'), \quad (10)$$

where

$$\rho(\mathbf{r} - \mathbf{r}') = \frac{\sigma^3}{\pi^{3/2}} \exp[-\sigma^2(\mathbf{r} - \mathbf{r}')^2] \quad (11)$$

is the smearing function, with  $\sigma$  as the smearing parameter. On the other hand, momentum dependent factors are introduced. For the smeared Coulomb-like and smeared spin-dependent term, the semirelativistic corrections are

$$\begin{aligned} \tilde{G}(r) &\rightarrow \left(1 + \frac{p^2}{E_1 E_2}\right)^{1/2} \tilde{G}(r) \left(1 + \frac{p^2}{E_1 E_2}\right)^{1/2}, \\ \tilde{V}_i(r) &\rightarrow \left(\frac{m_1 m_2}{E_1 E_2}\right)^{1/2+\epsilon_i} \tilde{V}_i(r) \left(\frac{m_1 m_2}{E_1 E_2}\right)^{1/2+\epsilon_i}, \end{aligned} \quad (12)$$

respectively.  $E_1$  and  $E_2$  represent the energies of the c-quark and  $\bar{c}$ -quark in charmonium, respectively. The correction factors,  $\epsilon_i$ , account for various types of hyperfine interactions, including spin-spin and tensor terms, as described in Ref. [24].

TABLE I: The parameters of the MGI model used in this work. These parameters are determined from our previous work [56].

Parameters	Values	Parameters	Values
$b$	0.2687 GeV <sup>2</sup>	$\epsilon_i$	0.012
$c$	-0.3673 GeV	$\epsilon_{\text{so(V)}}$	-0.053
$\mu$	0.15 GeV	$\epsilon_{\text{so(S)}}$	0.083
$\epsilon_c$	-0.084	$m_u$	0.22 GeV
$m_d$	0.22 GeV	$m_c$	1.65 GeV

Currently, the experimental understanding of high-lying charmonium remains relatively limited compared with light flavored mesons. The BESIII, Belle II, LHCb, and Super  $\tau$  Charm Facility (STCF) will be utilized to search for these high-lying charmonium states in the future and expand our comprehension of these undiscovered states. The subsequent section will discuss the most promising candidates for detection among these states.

In Ref. [56], we find that the  $Y(4200)$  can be treated as a good scaling point to construct high-lying charmonium states above 4 GeV in an unquenched quark potential model. Especially, two related  $^3D_1$  wave dominated charmonium partner states  $\psi(4380)$  and  $\psi(4500)$  are predicted. The analysis indicates that the reported vector  $Y$  states below 4.5 GeV can be well described under the  $S-D$  mixing scheme. Therefore, it is necessary to extend our study to predict the higher radial and orbital charmonium spectrum using the same model as that in Ref. [56].

The MGI model parameters adopted in this study are the same as those in Ref. [56], and they effectively reproduce the observed charmonium mass spectrum. These parameters are listed in Table I. The mass spectrum and spatial wave functions are determined by solving the Schrödinger equation with the MGI potential and the specified parameters. Here, we present numerical results for the masses, strong decay widths, and radiative decay widths of various charmonium states. We focus on charmonium states with orbital angular momentum  $L$  up to 4 and principal quantum number  $n$  up to 3, particularly on  $2D$  and  $1F$  states, where an unquenched model is required to account for screening effects.

The calculated charmonium mass spectrum is presented in Fig. 2, including the discussed states in our work and the low-lying states from our previous calculation [56]. We contrast our theoretical predictions from the MGI model with lattice QCD results [79] and experimental values. This investigation specifically focuses on states below the 4.2 GeV threshold, motivated by the abundant experimental data in this energy regime.

Our results indicate that the masses of the  $2D$  states are predicted to be around 4.12–4.14 GeV, which is approximately 70 MeV smaller than the values reported in Ref. [46]. The masses of  $1D$  states,  $3D$  states and  $2^3D_1$  state are close to the lattice QCD results [79]. For the  $2^3D_1$  state, the mass is 4125 MeV, which is smaller than the Particle Data Group (PDG) value of  $\psi(4160)$  [54]. The authors of Ref. [80] reevaluated the resonance parameters of  $\psi(4160)$  by analyzing the invariant mass spectrum of  $B^+ \rightarrow K^+ \mu^+ \mu^-$ . Their results indicate that the previous reported mass of  $\psi(4160)$  is overestimated. This conclusion is further supported by analyzing  $e^+e^- \rightarrow D_s \bar{D}_s^*$  and extracting the mass of  $\psi(4160)$  at  $4145.76 \pm 4.48$  MeV, which is consistent with our predicted mass for the  $2^3D_1$  state. It is worth mentioning that our result also aligns with the lattice QCD calculation of [79] (4138 MeV). The mass of the  $2^1D_2$  is identical to that of the  $2^3D_2$  at 4137 MeV, while the mass of the  $2^3D_3$  is 4144 MeV.

The masses of the  $1F$  states are almost degeneracy, approximately 4.07 GeV, which include 4074 MeV for  $1^1F_3$ , 4070 MeV for  $1^3F_2$ , 4075 MeV for  $1^3F_3$  and 4076 MeV for  $1^3F_4$ , respectively. Our results are consistent with the estimates provided in Ref. [46], while about 40 MeV smaller than the results of lattice QCD Ref. [79].

As shown in Fig. 2, the predicted masses of the four  $3D$  states are approximately 4.34 GeV, which are close with the results of lattice QCD [79]. For the  $2F$  states, we find masses around 4.29 GeV, which is different from those predicted by the quenched model in Ref. [46]. For the  $3F$  states, the MGI

model predicts masses around 4.45 GeV, and the masses of these states are nearly degeneracy. For all  $G$ -wave states, the masses are nearly identical for states with the same  $n$ . For the  $1G$  states, the masses are approximately 4.25 GeV, and the masses of the  $2G$  states are approximately 4.43 GeV. Regarding the  $3G$ -wave state, their masses are all around 4.54 GeV. When these high-lying states are with the same  $n$  and  $J^{PC}$ , masses of these states demonstrate almost degeneracy.

We observe that for the  $F$ -wave state with  $n = 1$ , the mass predictions from unquenched potential models are close to those from quenched models. However, for higher states such as the  $2D$  and  $1G$  states, unquenched models generally predict lower masses, highlighting a growing discrepancy between the two approaches. As the radial excitation  $n$  increases for the  $D$ -,  $F$ -, and  $G$ -wave states, these mass differences between unquenched and quenched models become more pronounced. This trend suggests that the screening effect intensifies with increasing quantum numbers  $L$  and  $n$ . These differences in mass spectra also impact the calculated strong decay widths, which we discuss in the following sections.

### III. STRONG DECAY

In the QPC model [71–74], the transition matrix for the  $A \rightarrow B + C$  process is written as  $\langle BC | \mathcal{T} | A \rangle = \delta^3(\mathbf{P}_B + \mathbf{P}_C) \mathcal{M}^{M_{J_A} M_{J_B} M_{J_C}}(\mathbf{P})$ , where  $\mathcal{M}^{M_{J_A} M_{J_B} M_{J_C}}(\mathbf{P})$  represents the helicity amplitude, and  $\mathbf{P}_B$  and  $\mathbf{P}_C$  are the momenta of mesons  $B$  and  $C$ , respectively, in the stationary reference frame of meson  $A$ . The states  $|A\rangle$ ,  $|B\rangle$ , and  $|C\rangle$  refer to the mock states associated with mesons  $A$ ,  $B$ , and  $C$ , respectively. The transition operator  $\mathcal{T}$  describes the quark-antiquark pair creation from the vacuum, and it has the form

$$\mathcal{T} = -3\gamma \sum_{m,i,j} \langle 1m; 1-m | 00 \rangle \int d\mathbf{p}_3 d\mathbf{p}_4 \delta^3(\mathbf{p}_3 + \mathbf{p}_4) \times \mathcal{Y}_{1m} \left( \frac{\mathbf{p}_3 - \mathbf{p}_4}{2} \right) \chi_{1,-m}^{34} \phi_0^{34}(\omega_0^{34})_{ij} b_{3i}^\dagger(\mathbf{p}_3) b_{4j}^\dagger(\mathbf{p}_4), \quad (13)$$

where the dimensionless constant  $\gamma$  describe the intensity of quark pairs  $u\bar{u}$ ,  $d\bar{d}$ , or  $s\bar{s}$  produced from the vacuum and can be determined from experimental data.<sup>1</sup> The state  $\chi_{1,-m}^{34}$  is a spin-triplet configuration, while  $\phi_0^{34}$  and  $\omega_0^{34}$  represent the SU(3) flavor and color singlets, respectively. The term  $\mathcal{Y}_{lm}(p) = |p|^l Y_{lm}(p)$  is the solid harmonic function.

<sup>1</sup> In fact, the parameters of the MGI model are determined by observed charmonium mass spectra, its confinement and static corrections arising from sea quark-antiquark pairs in the QCD vacuum. Crucially, this model does not explicitly include dynamical quark-pair creation or decay amplitudes. On the other hand, the QPC model describes the dynamical process of light quark-antiquark pair creation during two body strong decay. The quark-pair creation parameter  $\gamma$  is determined by fitting experimental partial decay widths of charmonium states, and is independent of the screened potential's spectroscopic inputs. Two models address separate observables (masses vs. decay widths) and their parameters are derived from entirely independent datasets.

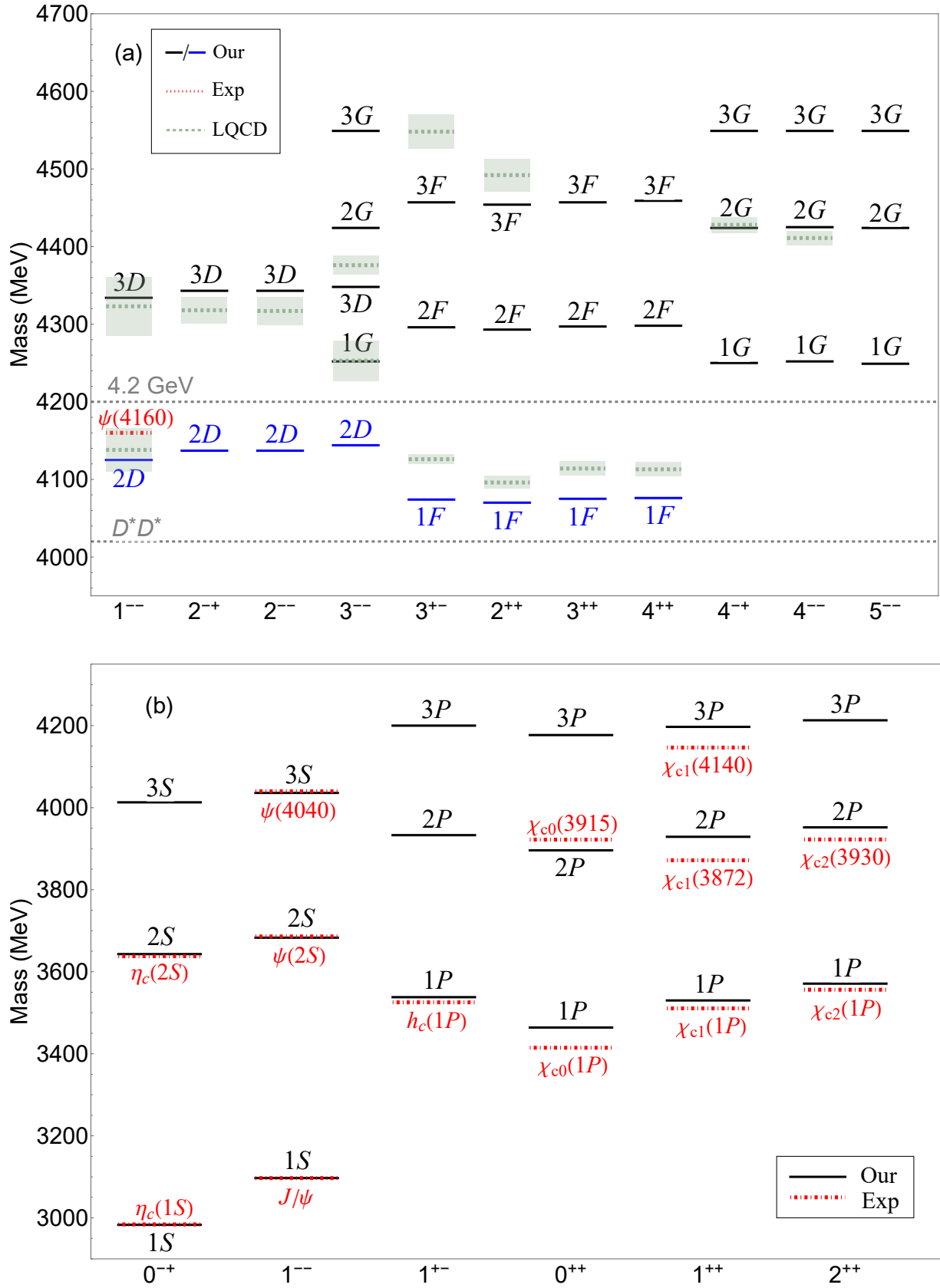


FIG. 2: Mass spectrum of  $D$ -,  $F$ -,  $G$ - wave charmonia and low-lying charmonia obtained in MGI model. The states marked by blue color represent the states we focused and the states marked by black color represent the states beyond 4.2 GeV and the states . The red dashed line represent the experimental values from PDG, and the green dashed line represent the result from lattice QCD [79]. The green bands mark the error range of lattice data. All the masses are given in units of MeV.



The helicity amplitude  $\mathcal{M}^{M_{J_A} M_{J_B} M_{J_C}}(\mathbf{P})$  can be related to the partial wave amplitude using the Jacob-Wick formula [81]:

$$\begin{aligned} \mathcal{M}^{JL}(A \rightarrow BC) &= \frac{\sqrt{4\pi(2L+1)}}{2J_A+1} \sum_{M_{J_B} M_{J_C}} \langle L0; JM_{J_A} | J_A M_{J_A} \rangle \\ &\times \langle J_B M_{J_B}; J_C M_{J_C} | J_A M_{J_A} \rangle \\ &\times \mathcal{M}^{M_{J_A} M_{J_B} M_{J_C}}(\mathbf{P}), \end{aligned} \quad (14)$$

where  $\mathbf{L}$  is the orbital angular momentum between the final states  $B$  and  $C$ , and  $\mathbf{J} = \mathbf{J}_B + \mathbf{J}_C$ . The general partial width for the  $A \rightarrow BC$  decay is

$$\Gamma_{A \rightarrow BC} = \frac{\pi}{4} \frac{|\mathbf{P}|}{m_A^2} \sum_{JL} |\mathcal{M}^{JL}(\mathbf{P})|^2, \quad (15)$$

where  $m_A$  is the mass of the parent meson  $A$ . The dimensionless parameter  $\gamma = 5.84$  is the same as in Ref. [56], and the strength for creating  $s\bar{s}$  from the vacuum satisfies the relation of  $\gamma_s = \gamma/\sqrt{3}$ .

For our calculations, we use the numerical spatial wave functions obtained in Section II as inputs. The numerical spatial wave functions of the final mesons are the same as those used in Refs. [65, 66]. The results of our calculations are presented in Table II.

#### A. The $2D$ and $1F$ states

Following the gradual discovery of the ground states of  $D$ -wave charmonium mesons, there is increasing optimism that the  $2D$  and  $1F$  states will be identified in future experimental efforts. Consequently, this work begins with an analysis of the decay properties of the predicted  $2D$  and  $1F$  states.

The masses of  $2D$  states and  $1F$  states are close to the  $D^*D^*$  threshold, therefore we present the decay behaviors of  $D$ -wave and  $F$ -wave states near open flavor threshold in Fig. 3 and Fig. 4. We set The mass axis spans  $\pm 150$  MeV about the central value. Compared with previous result of Ref. [58–60] from other unquenched model, the discrepancy between our results and other values does not exceed than 30 MeV. We therefore adopt the range of  $\pm 30$  MeV around the calculated value as estimate for the masses of the investigated states.

In our calculation, the  $2D$  states lie at approximately 4140 MeV, and their open decay channels as a function of the masses of  $2D$  states are shown in Fig. 3. From Table II, we observe that the two primary decay channels for the  $2^1D_2$  state are  $DD^*$  and  $D^*D^*$ , with the branching fraction reaching up to 98%. Therefore, we suggest that the  $2^1D_2$  state may be detected via these decay modes. When comparing our results to those in Ref. [46], we find that our decay widths are generally smaller. Notably, the  $D_sD_s^*$  decay mode is an order of magnitude smaller in our work than in Ref. [46].

For the  $J^{PC} = 1^{--}$  states with  $n = 2$ , the two dominant decay channels are  $DD$  and  $D^*D^*$ , with the  $DD^*$  process being suppressed, as shown in Fig. 3. In our calculations, the total decay width is 48.73 MeV while mass is 4125 MeV, with branching ratios of 39.81% and 56.78% for the  $DD$  and

$D^*D^*$  channels, respectively. The ratio of partial widths is  $\Gamma(DD) : \Gamma(D^*D^*) = 1.0 : 1.4$ . Although the decay modes of this state reported in Ref. [46] show a similar trend, there is a notable discrepancy in the total decay width, which they estimate to be 74 MeV. This difference may be attributed to our calculated mass of 4125 MeV, which is lower than their value of 4194 MeV. Furthermore, the decay widths for the  $D_sD_s$  and  $D_sD_s^*$  modes are significantly different: 0.04 MeV and 1.08 MeV in our work, compared to 8.0 MeV and 14 MeV in Ref. [46]. In our calculation, the width of  $D_sD_s$  and  $D_sD_s^*$  channels are less than 5 MeV in our mass regime.

The total width of  $2^1D_2$  state is 57.82 MeV while the mass is 4137 MeV. Its dominant decay channels are  $DD^*$  and  $D^*D^*$ , with decay widths of 22.88 MeV and 23.95 MeV, respectively. Their branching ratios are 50.97% and 46.96%. Compared to Ref. [46], our mass is 21 MeV lower, and our total decay width of 57.85 MeV corresponds to nearly half their value of 111 MeV. As shown in Fig. 3, the width of  $2^1D_2$  state can not fit the result of Ref. [46] in our mass regime. Specifically, for the  $D_sD_s^*$  decay mode, we predict a decay width of 1.2 MeV with a branching ratio of 2.08%, while Ref. [46] estimates a decay width of 18 MeV with a branching ratio of 16.22%.

For the  $2^3D_2$  state, the primary decay channels are  $DD^*$  and  $D^*D^*$ , with decay widths of 22.88 MeV and 23.95 MeV, respectively. Their branching ratios are 47.05% and 49.25%. Compared to Ref. [46], our mass is 21 MeV lower, and our total decay width of 48.63 MeV is significantly smaller than their value of 92 MeV. If we set the mass of  $2^3D_2$  is 4220 MeV, we can obtain the same decay width of the result in Ref. [46]. Specifically, for the  $D_sD_s^*$  decay mode, we predict a decay width of 1.8 MeV with a branching ratio of 3.7%, while Ref. [46] estimates a decay width of 26 MeV with a branching ratio of 28.26%. We observe that decay behaviors of  $2^1D_2$  and  $2^3D_2$  states are nearly identical, which may result from their identical masses.

The two main decay channels of the  $2^3D_3$  state are  $DD^*$  and  $D^*D^*$ , with branching ratios of 40.1% and 53.0%, respectively. The width of  $DD$  decay channel for the  $2^3D_3$  state is notably smaller than the value reported in Ref. [46], showing a difference of about one order of magnitude. However, the decay modes involving strange quarks remain consistent with those in the other  $2D$  states, and are similarly smaller than those reported in Ref. [46]. Despite slight differences in the calculated masses of the  $2D$  states, the decay modes and branching ratios are largely consistent. Furthermore, Fig. 3 demonstrates that the width of the  $2^3D_3$  state primarily depends on the  $D^*D^*$  channel across mass variations, whereas the  $DD^*$  and  $DD$  channels exhibit negligible mass dependence.

For the  $2^1D_2$ ,  $2^3D_2$ , and  $2^3D_3$  states, the dominant decay channels are  $DD^*$  and  $D^*D^*$ . However, compared to Ref. [46], the branching ratios for these two channels are notably higher in our study. On the other hand, decay modes involving strange quarks are less pronounced in our results, which highlights the need for further experimental validation. The masses of  $2D$  states reported in Ref. [46] are systematically lower than our predictions, this discrepancy can be attributed to unquenched effects in our MGI model. These unquenched

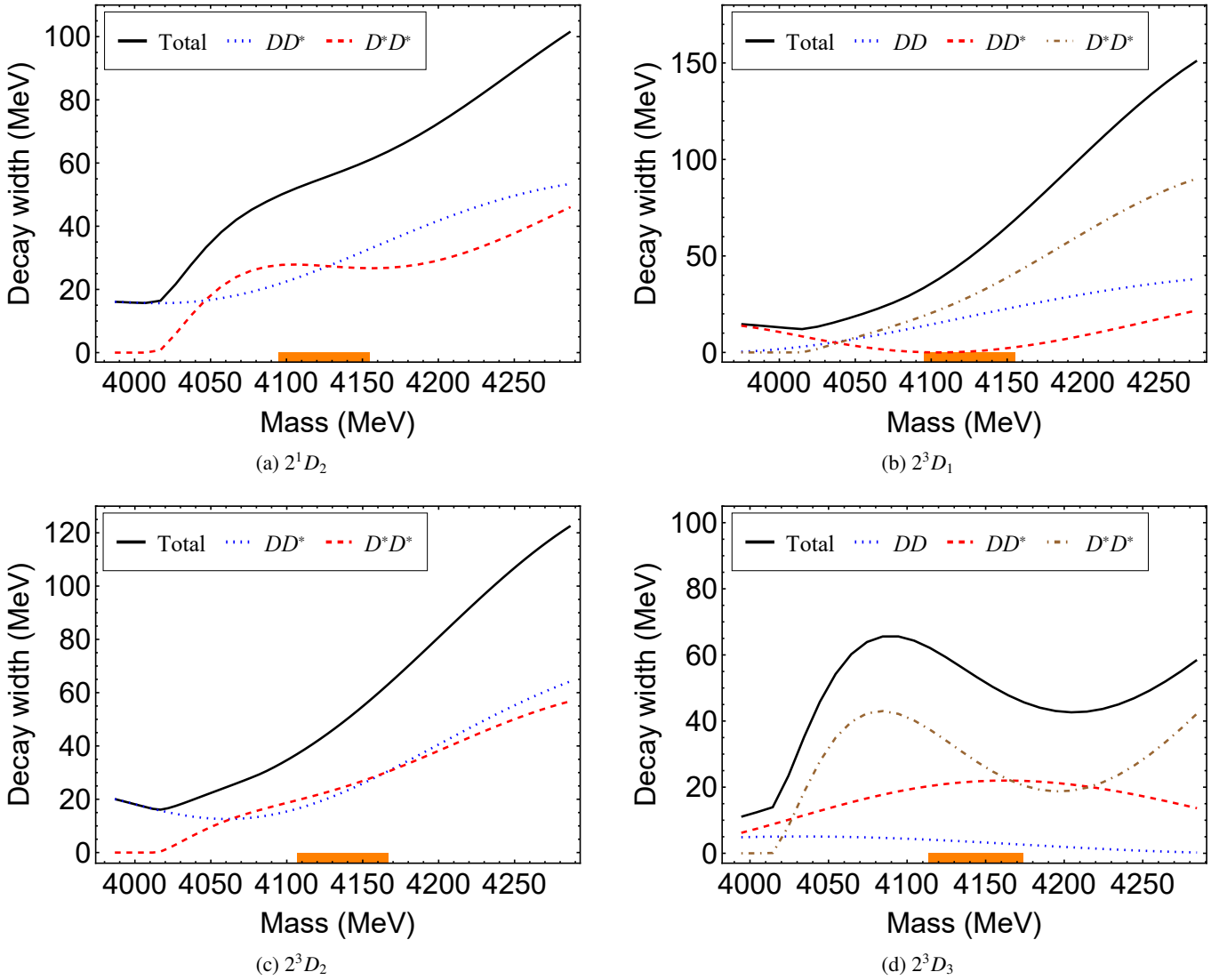


FIG. 3: Strong decay widths of the  $D$ -wave states near open flavor threshold. The mass axis indicates  $\pm 150$  MeV around our nominal value for the mass of these states. The channels with widths less than 5 MeV are not shown here, but their contributions are included in the total widths. The yellow band on the mass axis indicates  $\pm 30$  MeV around our calculated mass values.

effects result in fewer observed decay modes of  $2D$  states compared to the quenched model predictions, while the total decay width of these states is reduced by reducing the masses of high-lying states and making some decay channels inaccessible.

In Table II, we present the decay information for the  $F$  states with  $n = 1, 2, 3$ . Additionally, we present the major decay channels of  $1F$  states and their mass-dependent behaviors in Fig. 4. As the mass of  $1F$  states increases, the width of  $1F$  states also increases.

For the  $1^1F_3$  state, the dominant strong decay channel is  $DD^*$ , followed by  $D^*D^*$ , which also contributes notably. We predict the ratio of partial widths to be  $\Gamma(DD^*) : \Gamma(D^*D^*) = 6.2 : 1.0$ . However, Ref. [46] reports that the  $DD^*$  channel accounts for nearly the entire strong decay width in their calculations. The total width of  $1^1F_3$  is 78.78 MeV, close to the

result of Ref. [46]. As shown in Fig. 4, if the mass of  $1^1F_3$  state were increased to 4150 MeV, the total width would rise to 151 MeV, with the  $DD^*$  partial width reaching 55 MeV. This results  $\Gamma(DD^*) : \Gamma(D^*D^*)$  varies to 1.75 : 1.0.

Among these states, the broadest is the  $1^3F_2$  state, with a width of 112.48 MeV. The primary decay channels contributing to its width are  $DD$  and  $DD^*$ , which together account for 95% of the strong decay width. This result is in agreement with Ref. [46], although our findings show that the partial width of the  $DD^*$  channel is larger than that of the  $DD$  channel, which differs from the calculation in Ref. [46]. Similar to the  $1^1F_3$  state, the  $1^3F_3$  state also exhibits  $DD^*$  as the dominant strong decay channel, contributing 92% to the total width, with the  $D^*D^*$  channel being relatively suppressed. From Fig. 4, when the mass of  $1^3F_2$  state varies from 4050 MeV to 4150 MeV, the partial width of  $D^*D^*$  channel re-

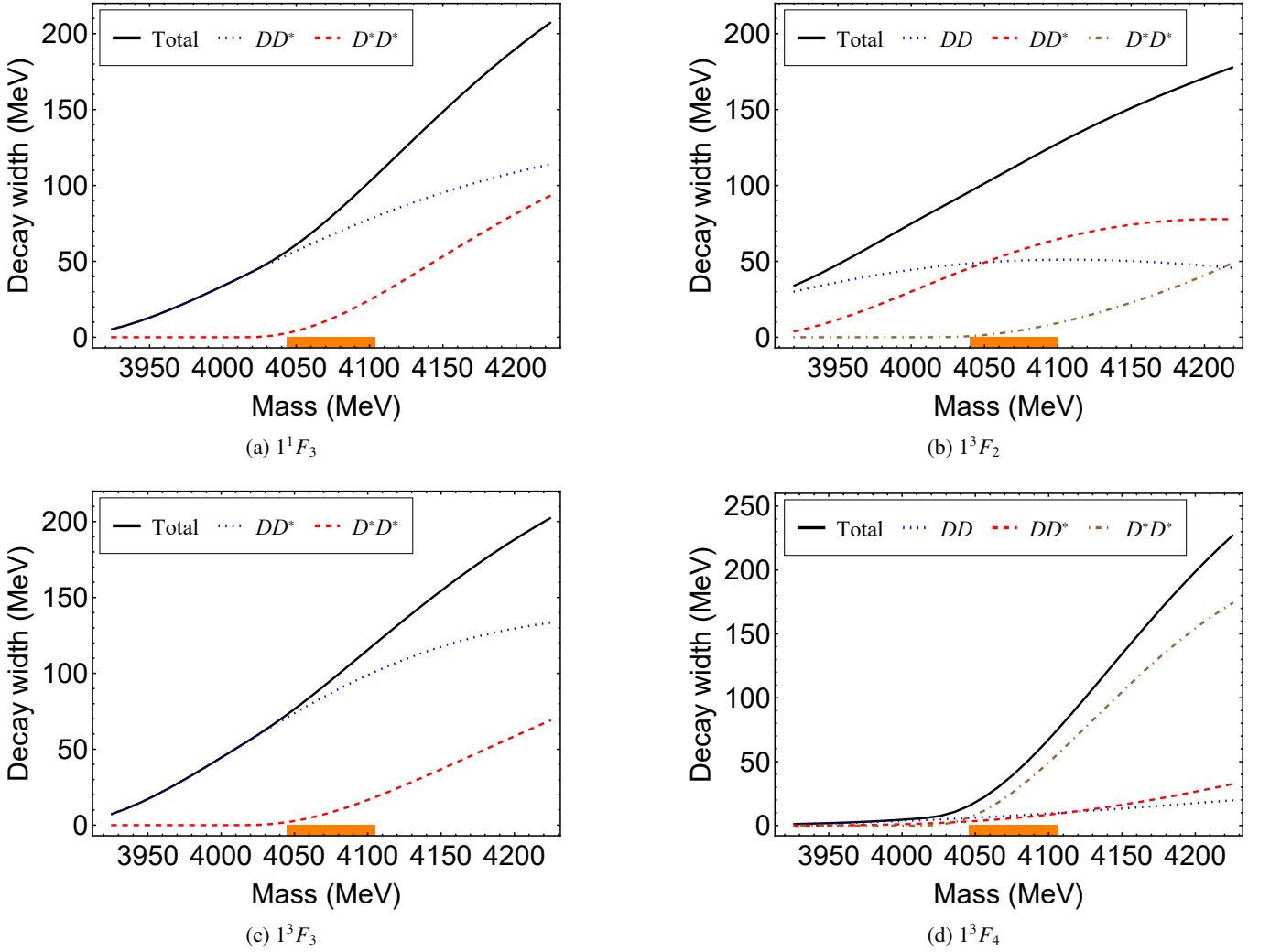


FIG. 4: Strong decay widths of the  $1F$  states near open flavor threshold. The mass axis indicates  $\pm 150$  MeV around our nominal value for the mass of this states. The channels with widths less than 5 MeV are not shown here, but their contributions are included in the total widths. The yellow band on the mass axis indicates  $\pm 30$  MeV around our calculated mass values.

mains subdominant compared to other two primary channels. It represent the  $D^*D^*$  channel contributes fewer decay width to  $1^3F_2$  state relative to other  $1F$  states.

The  $1^3F_4$  state is a narrow state, with a strong decay width of 37.97 MeV, which is larger than the estimated width of 8.6 MeV reported in Ref. [46]. The  $1^3F_4$  state predominantly decays into the  $DD$ ,  $DD^*$ , and  $D^*D^*$  channels, with a partial width ratio of  $\Gamma(DD) : \Gamma(DD^*) : \Gamma(D^*D^*) = 1.4 : 1.0 : 4.0$ . This ratio differs from that reported in Ref. [46], where smaller phase spaces in the  $D^*D^*$  decay mode lead to narrower partial widths. Additionally, this mass discrepancy may influence the widths of other decay channels. Fig. 4 reveals that the width of the  $1^3F_4$  state depends significantly on the  $D^*D^*$  channel. When the  $D^*D^*$  channel opens, the width obviously increases. For example, the width of  $1^3F_4$  state is from 11.6 MeV at  $M = 4055$  MeV to 66.6 MeV at  $M = 4155$  MeV. This sharp threshold dependence highlights the necessity of precisely determining the mass of  $1^3F_4$  state.

## B. Other high-lying charmonia

The dominant decay channels for the  $3^1D_2$  state remain  $DD^*$  and  $D^*D^*$ . We predict the branching ratios for these channels to be 63.17% and 23.77%, respectively. Additionally, the  $DD_2^*$  channel exhibits a greater decay width compared to the  $DD_0^*$ ,  $DD_1$ , and  $DD_1'$  channels. The  $3^1D_2$  state also shows three decay processes involving strange quarks, with the  $D_s D_{s0}$  channel contributing the largest decay width (3.22%) due to its higher mass threshold. The  $3^3D_1$  state has three primary decay channels:  $DD$ ,  $D^*D^*$ , and  $DD_1'$ , with the ratios of partial widths predicted to be  $\Gamma(DD) : \Gamma(D^*D^*) : \Gamma(DD_1') = 1.9 : 1.7 : 1.0$ . Compared to the  $2^3D_1$  state, the  $DD^*$  and  $D^*D^*$  channels remain dominant, but the new  $DD_1'$  channel contributes a branching ratio of 18.76%. For the  $3^3D_2$  state, the  $DD^*$  channel dominates, with a branching ratio higher than that of the  $D^*D^*$  channel, which contrasts with the  $2^3D_2$  state, where  $D^*D^*$  dominates. This state primarily de-



cays into  $DD^*$ ,  $D^*D^*$ ,  $DD_1$ ,  $DD'_1$ , and  $DD_2^*$ , with the ratio of partial widths predicted to be  $\Gamma(DD^*) : \Gamma(D^*D^*) : \Gamma(DD_1) : \Gamma(DD'_1) : \Gamma(DD_2^*) = 9.2 : 4.9 : 1.1 : 1.2 : 1.0$ . Finally, for the  $3^3D_3$  state, the most significant decay channel is  $DD^*$ , with a branching ratio of 51.2%. Compared to the  $2^3D_3$  state, the partial decay width of the  $3^3D_3$  state into the  $D^*D^*$  channel decreases significantly, primarily due to the node effect in the corresponding spatial wave function.

The strong decay width of the  $2^1F_3$  state is approximately 38.78 MeV, and it predominantly decays into  $DD^*$  and  $D^*D^*$ , with  $DD_0^*$ ,  $D_sD_s^*$ , and  $D_s^*D_s^*$  channels being relatively suppressed. The ratio between the main decay channels is predicted to be  $\Gamma(DD^*) : \Gamma(D^*D^*) = 2 : 1$ . The  $2^3F_2$  state has its decay width primarily contributed by the  $DD$ ,  $DD^*$ , and  $D^*D^*$  modes, with a corresponding partial width ratio of  $\Gamma(DD) : \Gamma(DD^*) : \Gamma(D^*D^*) = 1.2 : 1.0 : 1.1$ . The  $2^3F_3$  state exhibits two dominant decay modes:  $DD^*$  and  $D^*D^*$ , with a predicted partial width ratio of  $\Gamma(DD^*) : \Gamma(D^*D^*) = 2.4$ . The narrowest of the  $2F$  states is the  $2^3F_4$  state, which primarily decays into the  $D^*D^*$  channel, with the branching fraction reaching 85.12%. Similar to the  $2D$  states, decay modes involving strange quarks in the  $2F$  states are less prominent in our results. The decay channels  $DD^*$  and  $D^*D^*$  account for nearly the entire decay width of the  $2^1F_3$ ,  $2^3F_3$ , and  $2^3F_4$  states, which contrasts sharply with the results from Ref. [46], where multiple decay channels exhibit significant branching ratios. This difference is likely due to unquenched effects in our model.

The primary decay channels for  $3F$  states remain  $DD^*$  and  $D^*D^*$ , but with increasing mass, new decay channels become accessible. The  $3^1F_3$  state has two dominant decay channels,  $DD^*$  and  $D^*D^*$ , with the  $DD_2^*$  channel also contributing significantly. The predicted ratio of partial widths is  $\Gamma(DD^*) : \Gamma(D^*D^*) : \Gamma(DD_2^*) = 2.8 : 1.6 : 1.0$ . The decay width of the  $3^3F_2$  state is governed by the  $DD$ ,  $DD^*$ ,  $D^*D^*$ , and  $DD_1$  channels, with the branching fraction  $\text{Br}[\chi_{c2}(3^3F_2) \rightarrow DD, DD^*, D^*D^*, DD_1]$  reaching up to 92%. The  $3^3F_3$  state has three dominant decay modes:  $DD^*$ ,  $D^*D^*$ , and  $DD_2^*$ , with the ratio of partial widths predicted to be  $\Gamma(DD^*) : \Gamma(D^*D^*) : \Gamma(DD_2^*) = 2.7 : 1.3 : 1.0$ . Finally, the  $3^3F_4$  state predominantly decays into  $DD^*$  and  $D^*D^*$ , with the ratio between partial widths being approximately  $\Gamma(DD^*) : \Gamma(D^*D^*) = 1.0 : 4.1$ . The decay pattern for the  $3F$  states closely follows that of the  $1F$  and  $2F$  states, with the  $DD^*$  channel remaining dominant.

In Table II, we present the strong decay widths for the  $1^3G_3$ ,  $2^3G_3$ , and  $3^3G_3$  states. As a result, the strong decay widths of these states are similar, their dominant decay channels are  $DD^*$  and  $D^*D^*$ . Due to the near equivalence in mass among these states, their strong decay widths are similar, although the ratios of the partial widths differ. The total decay widths of the  $1G$  states are approximately equal, while the ratios between the partial widths of  $DD^*$  and  $D^*D^*$  vary. Specifically, for the  $1^1G_4$  state, the ratio is  $\Gamma(DD^*) : \Gamma(D^*D^*) = 1.4 : 1.0$ , while for the  $1^3G_4$  state, it is  $\Gamma(DD^*) : \Gamma(D^*D^*) = 1.9 : 1.0$ , and for the  $1^3G_5$  state, the ratio is  $\Gamma(DD^*) : \Gamma(D^*D^*) = 1.6 : 8.0$ . When compared to the results in Ref. [46], we find that the  $DD^*$  and  $D^*D^*$  channels remain the dominant decay modes

across all  $1G$  states. However, Ref. [46] reports that the  $DD$  channel contributes more significantly to the decay width, particularly for the  $1^3G_3$  and  $1^3G_5$  states. In fact, the width of the  $DD$  channel significantly exceeds that of the  $D^*D^*$  channel for the  $1^3G_3$  state, which contrasts with our findings. This discrepancy may stem from differences in the wave function for the  $D^*$  meson used in our calculation, which is based on the MGI model, as opposed to the simple harmonic oscillator (SHO) wave function employed in Ref. [46].

The decay behaviors of  $2G$  states are closely resemble those of the  $G$  states. The dominant decay channels for the  $2^1G_4$  and  $2^3G_4$  states remain  $DD^*$  and  $D^*D^*$ . However, the open-charm decay channels  $DD_0^*$ ,  $DD_1$ ,  $DD'_1$ ,  $DD_2^*$ , and  $D^*D_0^*$  are relatively suppressed. The ratios of the main partial widths for the  $2^1G_4$  and  $2^3G_4$  states are  $\Gamma(DD^*) : \Gamma(D^*D^*) = 1.6$  and  $\Gamma(DD^*) : \Gamma(D^*D^*) = 2.5$ , respectively. In addition to the  $DD^*$  and  $D^*D^*$  modes, the  $DD$  channel exhibits a considerable branching ratio for the  $2^3G_3$  state. The partial width ratios of the dominant channels for the  $2^3G_3$  state are  $\Gamma(DD) : \Gamma(DD^*) : \Gamma(D^*D^*) = 2.2 : 3.3 : 1.0$ . For both the  $2^3G_3$  and  $3^3G_3$  states, the  $DD^*$  decay channel exhibits the largest partial width. Among the  $2G$  states, the  $2^3G_5$  state is the narrowest. Its decays are dominated by the  $DD$  and  $D^*D^*$  channels, with a corresponding partial width ratio of  $\Gamma(DD) : \Gamma(D^*D^*) = 1.0 : 11.4$ . Additionally, channels involving strange quarks also contribute to the decay widths. For example, the  $D_sD_s^*$  channel contributes to the widths of the  $2^1G_4$ ,  $2^3G_3$ , and  $2^3G_4$  states, while the  $D_sD_s$  channel contributes to the  $2^3G_3$  state. However, these contributions to the total widths are negligible.

The channel with the largest decay widths is  $DD^*$  for the  $3^1G_4$ ,  $3^3G_3$ , and  $3^3G_4$  states, while the  $D^*D^*$  channel is dominant for the  $3^3G_5$  state. Although the  $DD^*$  and  $D^*D^*$  channels are still the dominant decay channels for all  $3G$  states, their branching ratios are smaller than those of the corresponding  $2G$  states. The corresponding ratios of  $3^1G_4$  and  $3^3G_4$  states between main partial widths are  $\Gamma(DD^*) : \Gamma(D^*D^*) = 1.5$  and  $\Gamma(DD^*) : \Gamma(D^*D^*) = 2.3$ , respectively. The decay rates into  $DD_0^*$ ,  $DD_2^*$ ,  $D^*D'_1$  and  $D^*D_2^*$  channels are also sizable for  $3^1G_4$  and  $3^3G_4$  states, with the branching fractions of  $\text{Br}[\psi(3^1G_4)/\psi(3^3G_4) \rightarrow DD_0^*, DD_2^*, D^*D'_1, D^*D_2^*]$  around 20%. The  $3^3G_3$  state mainly decays into  $DD, DD^*, D^*D^*, DD_1$ , and  $D^*D_1$ . Other open charm decay channels are relatively suppressed. The predicted ratio between the dominant partial widths in the MGI model is  $\Gamma(DD) : \Gamma(DD^*) : \Gamma(D^*D^*) : \Gamma(DD_1) : \Gamma(D^*D_1) = 4.4 : 5.9 : 2.5 : 1.6 : 1.0$ . The branching ratio of the  $DD$  channel for  $3^3G_3$  state is 24.38%, which is larger than that of the  $D^*D^*$  channel, similar to the  $2^3G_3$  state. The  $3^3G_5$  state is narrowest  $3G$  state with the width 23 MeV. The branching ratios of the  $DD$  and  $DD^*$  decay channels are smaller, while the  $D^*D^*$  and  $D^*D_2^*$  channels dominate. The ratio between the main partial widths is  $\Gamma(D^*D^*) : \Gamma(D^*D_2^*) = 5 : 1$ .

#### IV. RADIATIVE DECAY

In this section, we briefly outline the model used to calculate radiative decay. The quark-photon electromagnetic coupling is described by

$$H_e = - \sum_j e_j \bar{\psi}_j \gamma_\mu^j A^\mu(\mathbf{k}, \mathbf{r}) \psi_j, \quad (16)$$

where  $\psi_j$  is the  $j$ -th quark field with a charge  $e_j$  in a hadron, and  $\mathbf{k}$  denotes the 3-momentum of the photon.

The spatial wave functions are calculated using the potential models outlined in Sec. II. The nonrelativistic expansion of  $H_e$  can be written as [59, 82–86]

$$h_e \simeq \sum_j \left[ e_j \mathbf{r}_j \cdot \boldsymbol{\epsilon} - \frac{e_j}{2m_j} \boldsymbol{\sigma}_j \cdot (\boldsymbol{\epsilon} \times \hat{\mathbf{k}}) \right] e^{-i\mathbf{k} \cdot \mathbf{r}_j}, \quad (17)$$

where  $\boldsymbol{\sigma}_j$ ,  $m_j$ , and  $\mathbf{r}_j$  stand for Pauli spin vector, the constituent mass and the coordinate for the  $j$ -th quark, respectively. The vector  $\boldsymbol{\epsilon}$  is the polarization vector of the photon. The standard helicity transition amplitude  $\mathcal{A}_\lambda$  between the initial state  $|J_i \lambda_i\rangle$  and the final state  $|J_f \lambda_f\rangle$  is given by

$$\mathcal{A}_\lambda = -i \sqrt{\frac{\omega_\gamma}{2}} \langle J_f \lambda_f | h_e | J_i \lambda_i \rangle, \quad (18)$$

where  $\omega_\gamma$  is the photon energy.  $J_f$  and  $J_i$  are the total angular momenta of the final and initial mesons, respectively, and  $\lambda_f$  and  $\lambda_i$  are the components of their total angular momentum along the  $z$  axis. In our calculations, we choose the initial hadron-rest frame for the radiative decay process, so that the momentum of the initial hadron is  $\mathbf{P}_i = 0$ , and the final hadron's momentum is  $\mathbf{P}_f = -\mathbf{k}$ . We set the polarization vector of the photon as  $\boldsymbol{\epsilon} = -\frac{1}{\sqrt{2}}(1, i, 0)$ , with the photon momentum directed along the  $z$  axial ( $\mathbf{k} = k\hat{\mathbf{z}}$ ).

The partial decay widths for the electromagnetic transitions are given by

$$\Gamma = \frac{|\mathbf{k}|^2}{\pi} \frac{2}{2J_i + 1} \frac{M_f}{M_i} \sum_\lambda |\mathcal{A}_\lambda|^2, \quad (19)$$

where  $J_i$  is the total angular momenta of the initial mesons, and  $M_i$  and  $M_f$  are the masses of the initial and final charmonium states, respectively. The electromagnetic transition rates we calculated are presented in Tables III and IV.

The numerical results indicate that the decay widths of  $D$ -wave states for transitions to  $P$ -wave and  $F$ -wave states are generally larger, whereas those to  $S$ -wave and  $D$ -wave states are comparatively smaller.

For the  $2^1D_2$  state, the dominant radiative decay channels are  $2^1D_2 \rightarrow 2^1P_1\gamma$  and  $1^1P_1\gamma$ , with decay widths of 167.10 keV and 58.45 keV, respectively. For the  $2^3D_1$  state, the largest radiative decay width corresponds to the  $2^3D_1 \rightarrow 2^3P_0\gamma$  channel, with a value of 126.39 keV. Other notable decay channels for this state include  $2^3D_1 \rightarrow 2^3P_1\gamma$  and  $1^3P_0\gamma$ , with widths of 115.98 keV and 82.20 keV, respectively. Table III shows that the largest decay width for the

$2^3D_2$  state occurs for the  $2^3D_2 \rightarrow 2^3P_1\gamma$  channel, with a width of 127.69 keV. The dominant decay channel for the  $2^3D_3$  state is  $2^3D_3 \rightarrow 2^3P_2\gamma$ , with a decay width of 212.66 keV, while other decay channels for this state are significantly smaller.

Regarding the  $F$ -wave states, we observe from Tables III and IV that their primary electromagnetic decay channel is to  $D$ -wave states. However, transitions to  $S$ -wave and  $G$ -wave states also exhibit decay widths on the order of keV.

For the  $1F$  states, the decay channels with the largest widths follow a trend similar to that of the  $D$ -wave states. For instance, the most significant decay channel for the  $1^3F_2$  state is  $1^3F_2 \rightarrow 1^3D_1\gamma$ , with a decay width of 439.69 keV, which is notably large. For the  $1^1F_3$ ,  $1^3F_3$ , and  $1^3F_4$  states, the major decay channels are to  $1^1D_2\gamma$ ,  $1^3D_2\gamma$ , and  $1^3D_3\gamma$ , with decay widths of 249.14 keV, 295.43 keV, and 269.26 keV, respectively. Notably, the strong decay width of the  $1^3F_2$  state in our calculations is 112.48 MeV, meaning the branching ratio for the  $1^3F_2 \rightarrow 1^3D_1\gamma$  channel is approximately 0.4%. This could be detectable in future experiments. Similarly, the branching ratio for the  $2D \rightarrow 2P\gamma$  channel is also significant. Since the  $2^3D_2$ ,  $2^1D_2$ , and  $2^3D_3$  states have not yet been observed, we suggest further investigation into the radiative decay channels involving the  $2P$  states.

The radiative decay behaviors of  $2D$  states and  $3D$  states are almost identical. The  $2F$  and  $3F$  states follow the same pattern as the  $1F$  states, but as the principal quantum number  $n$  increases, the radiative decay widths decrease.

Our results reveal that the broadest partial radiative widths correspond to transitions where both the initial and final states have the same quantum numbers  $n$  and  $S$  for  $D$  and  $F$  states.

#### V. DISCUSSION AND SUMMARY

Our understanding of the high-lying states within the charmonium family remains limited. With the recent observation of charmonium states above 4 GeV, we seize the opportunity to investigate the high-lying charmonium family. This includes a mass spectrum analysis using the MGI model, followed by two-body strong decay calculations within the framework of the QPC model, along with an analysis of radiative decays. This theoretical approach allows us to derive the resonance parameters for the charmonium states discussed, providing valuable insights for future research in heavy hadron spectroscopy.

In this study, we have calculated the mass spectrum for  $2D$ ,  $1F$ , and other high-lying charmonium states, incorporating unquenched effects by introducing a screening potential. Additionally, we provide a detailed analysis of the strong decay properties of these states, including several key decay channels and partial decay widths that are crucial for the identification of potential charmed meson candidates in upcoming experiments. We also investigate the radiative decay behaviors and highlight the primary radiative decay channels for the states considered.

Based on the aforementioned characteristics of high-lying charmonia, we analyze their production mechanisms qualitatively, with a particular focus on those states whose mass is

below 4.2 GeV. Given that the  $1D$  triplet and the  $2^3D_1$  state have already been observed among  $D$ -wave states, it is logical to explore potential experimental avenues for detecting the  $2^3D_2$  and  $2^3D_3$  states. Considering that these states have relatively narrow widths and their main decay channels are  $D^*D$  and  $D^*D^*$ , we expect to search for them experimentally in the  $D^*D$  and  $D^*D^*$  channels. As a reference, the  $1^3D_2$  state,  $\psi_2(3823)$ , was previously discovered in  $B \rightarrow \chi_{c1}\gamma K$  and  $B^+ \rightarrow J/\psi\pi^+\pi^-K^+$  processes [87, 88]. Similarly, the  $2^3D_2$  and  $2^3D_3$  states may potentially be observed through the  $B \rightarrow D^*DK$  and  $B \rightarrow D^*D^*K$  processes in further experiments such as those conducted by the LHCb and Belle II collaborations. However, the LHCb collaboration recently analyzed the  $B \rightarrow D^*DK$  process [50], and unfortunately, no evidence for the  $2^3D_2$  and  $2^3D_3$  states was found. We hope that more precise data in the future will help us discover these states.

In addition to  $B$ -meson decay processes, the hidden-charm decays of higher excited  $1^{--}$  charmonia produced directly from  $e^+e^-$  annihilation, also offer promising pathways for searching for the  $2^3D_2$  and  $2^3D_3$  states. For example, processes like  $e^+e^- \rightarrow \psi \rightarrow \pi^+\pi^-D^*D^{(*)}$  and  $e^+e^- \rightarrow \psi \rightarrow \eta D^*D^{(*)}$  could provide valuable opportunities for their detection. However, a rough estimate indicates that the mass of such a  $\psi$  state is likely to be above 4.7 GeV. Moreover, the mass gap of the  $2^3D_2$  and  $2^3D_3$  states is approximately 7 MeV in our results. Distinguishing these two states will require higher statistics to accurately measure their spins. These pose significant challenges for experiments at the upgraded BESIII and Belle II.

The successful identification of the  $1D$  triplet in charmonia motivates us to further explore the production mechanisms of states with higher orbital angular momentum, such as the  $1F$  triplet. Though the masses of  $1F$  triplet are quite close, their main decay channels are different. Based on the branching ratios of the open charm decay channel for the  $1F$  triplet shown in Table II, we propose that the  $1^3F_2$  state can be probed in the  $DD$  channel, while the  $1^3F_4$  state can be investigated in the  $D^*D^*$  channel. Since both  $1^3F_2$  state and  $1^3F_3$  state have significant branching ratios for  $D^*D$  channel, distinguishing between them in the  $D^*D$  channel remains a challenging task.

Analogous to the  $2^3D_2$  and  $2^3D_3$  states, the  $1F$  charmonia

triplet can be systematically investigated through two potential approaches: (1)  $B$ -meson decay processes and (2) hidden-charm decay channels of higher excited  $1^{--}$  charmonia. Furthermore, the C-even nature of the  $1F$  triplet enables its production via radiative transitions from these excited vector charmonia with mass above 4.2 GeV. Notably, the  $1^3F_2$  state with  $J^{PC} = 2^{++}$  emerges as a prime candidate for  $S$ -wave-dominated radiative transitions from excited vector charmonium states ( $1^{--}$ ). Therefore, we encourage that experimental collaborations, such as BESIII and Belle II, can pay attention to  $e^+e^- \rightarrow \gamma D\bar{D}$  process to search for the  $1^3F_2$  state in the future.

In conclusion, although the observations of the high-lying charmonium are filled with challenges, there are still promising opportunities for detecting these elusive states in the future, such as  $B \rightarrow D^*D^*K$ ,  $e^+e^- \rightarrow \pi\pi D^*D^{(*)}$  and  $e^+e^- \rightarrow \gamma DD$ . The ongoing and upcoming experiments, such as the upgraded BESIII, Belle II, LHCb, as well as future facility STCF, are expected to provide more precise data and higher statistics. These advancements will significantly enhance our ability to explore the high-lying charmonium sector.

We are currently entering a new era of high-precision hadron spectroscopy, driven by the upgrades to the Large Hadron Collider (LHC), the operation of Belle II, and the planned upgrades for the Beijing Electron Positron Collider (BEPC). The theoretical insights presented in this work regarding high-lying charmonium mesonic states may provide important guidance for experimental studies at BESIII and other upcoming facilities.

## ACKNOWLEDGMENTS

This work is supported by the National Natural Science Foundation of China under Grant Nos. 12335001 and 12247101, the ‘111 Center’ under Grant No. B20063, the Natural Science Foundation of Gansu Province (No. 22JR5RA389, No. 25JRRA799), the fundamental Research Funds for the Central Universities, and the project for top-notch innovative talents of Gansu province.

- 
- [1] J. J. Aubert *et al.* (E598), Experimental observation of a heavy particle  $J$ , *Phys. Rev. Lett.* **33**, 1404 (1974).
  - [2] J. E. Augustin *et al.* (SLAC-SP-017), Discovery of a narrow resonance in  $e^+e^-$  annihilation, *Phys. Rev. Lett.* **33**, 1406 (1974).
  - [3] G. S. Abrams *et al.*, The discovery of a second narrow resonance in  $e^+e^-$  annihilation, *Phys. Rev. Lett.* **33**, 1453 (1974).
  - [4] T. Himel *et al.*, Observation of the  $\eta_c(2980)$  produced in the radiative decay of the  $\psi'(3684)$ , *Phys. Rev. Lett.* **45**, 1146 (1980).
  - [5] C. Edwards *et al.*, Observation an an  $\eta'_c$  Candidate State with Mass  $3592 \pm 5$  MeV, *Phys. Rev. Lett.* **48**, 70 (1982).
  - [6] G. Goldhaber *et al.*,  $D$  and  $D^*$  Meson Production Near 4-GeV in  $e^+e^-$  Annihilation, *Phys. Lett. B* **69**, 503 (1977).
  - [7] J. Siegrist *et al.*, Observation of a resonance at 4.4-GeV and additional structure near 4.1-GeV in  $e^+e^-$  annihilation, *Phys. Rev. Lett.* **36**, 700 (1976).
  - [8] T. A. Armstrong *et al.*, Observation of the P-wave singlet state of charmonium, *Phys. Rev. Lett.* **69**, 2337 (1992).
  - [9] C. J. Biddick *et al.*, Inclusive gamma-Ray Spectra from  $\psi(3095)$  and  $\psi'(3684)$ , *Phys. Rev. Lett.* **38**, 1324 (1977).
  - [10] W. M. Tanenbaum *et al.*, Observation of an intermediate state in  $\psi'(3684)$  radiative cascade decay, *Phys. Rev. Lett.* **35**, 1323 (1975).
  - [11] J. S. Whitaker *et al.*, Radiative decays of  $\psi(3095)$  and  $\psi'(3684)$ , *Phys. Rev. Lett.* **37**, 1596 (1976).
  - [12] P. A. Rapidis *et al.*, Observation of a resonance in  $e^+e^-$  annihilation just above charm threshold, *Phys. Rev. Lett.* **39**, 526 (1977), [Erratum: *Phys.Rev.Lett.* 39, 974 (1977)].
  - [13] E. Eichten, K. Gottfried, T. Kinoshita, J. B. Kogut, K. D. Lane,

$2^1D_2$			$2^3D_1$			$2^3D_2$			$2^3D_3$			$1^3F_3$			$1^3F_2$		
Our	Ref. [46]		Our	Ref. [46]		Our	Ref. [46]		Our	Ref. [46]		Our	Ref. [46]		Our	Ref. [46]	
$\Gamma_{thy}$	$\Gamma_{thy}$	Br	$\Gamma_{thy}$	$\Gamma_{thy}$	Br	$\Gamma_{thy}$	$\Gamma_{thy}$	Br	$\Gamma_{thy}$	$\Gamma_{thy}$	Br	$\Gamma_{thy}$	$\Gamma_{thy}$	Br	$\Gamma_{thy}$	$\Gamma_{thy}$	Br
4137	4158		4125	4159		4137	4158		4144	4167		4074	4026		4070		
DD	DD	Br	DD	DD	Br	DD	DD	Br	DD	DD	Br	DD	DD	Br	DD	DD	Br
29.47	50.97%	50	19.4	39.81%	16	22.88	47.05%	34	3.27	6.03%	24	16.22%	24	16.22%	50.51	44.91%	98
27.15	46.96%	43	27.67	56.78%	35	23.95	49.25%	32	21.77	40.11%	50	33.78%	61	99.84%	56.37	50.12%	57
1.2	2.08%	18	1.08	2.22%	14	1.8	3.70%	26	0.36	0.66%	5.7	3.85%	0.1	0.16%	3.43	3.05%	0.1
57.82	100%	111	48.73	100%	74	48.63	100%	92	0.09	0.17%	1.2	0.81%	148	100%	2.17	1.93%	5.9
									54.27	100%					112.48	100%	161
$1^3F_3$			$1^3F_4$			$1^3G_4$			$1^3G_3$			$1^3G_2$			$1^3G_1$		
Our	Ref. [46]		Our	Ref. [46]		Our	Ref. [46]		Our	Ref. [46]		Our	Ref. [46]		Our	Ref. [46]	
$\Gamma_{thy}$	$\Gamma_{thy}$	Br	$\Gamma_{thy}$	$\Gamma_{thy}$	Br	$\Gamma_{thy}$	$\Gamma_{thy}$	Br	$\Gamma_{thy}$	$\Gamma_{thy}$	Br	$\Gamma_{thy}$	$\Gamma_{thy}$	Br	$\Gamma_{thy}$	$\Gamma_{thy}$	Br
4075	4029		4076	4021		4250	4225		4252	4237		4252	4228		4249	4214	
DD	DD	Br	DD	DD	Br	DD	DD	Br	DD	DD	Br	DD	DD	Br	DD	DD	Br
87.57	92.01%	83	8.12	21.39%	6.8	50.3	57.21%	72	19.34	24.28%	63	40.65%	63	40.65%	8.32	9.43%	10
7.6	7.99%	0.2	23.88	62.89%	0.05	36.46	41.47%	24	36.39	45.68%	66	42.58%	88	79.28%	12.91	14.64%	6.4
0.2	0.24%	0.2	0.04	0.11%	0.02	0.01	0.01%	0.01	21.23	26.65%	13	8.39%	19	17.12%	66.76	75.70%	41
0.04	0.08%	8	0.04	0.08%	8	0.01	0.01%	0.01	0.04	0.08%	8	0.04	0.08%	8	0.04	0.08%	8
1.08	16.22%	18	1.08	2.22%	14	1.14	1.30%	3	1.63	2.05%	10	6.45%	10	6.45%	0.15	0.17%	0.4
57.82	100%	111	48.73	100%	74	48.63	100%	92	1.08	1.36%	3	1.94%	3	1.94%	0.04	0.05%	0
									0.01	0.01%	0.01	0.00%	0	0.00%	0.01	0.01%	0
									87.92	100%					88.31	100%	58
$2^1F_3$			$2^1F_2$			$2^1F_4$			$2^3F_4$			$3^3D_1$			$3^3D_2$		
Our	Ref. [46]		Our	Ref. [46]		Our	Ref. [46]		Our	Ref. [46]		Our	Ref. [46]		Our	Ref. [46]	
$\Gamma_{thy}$	$\Gamma_{thy}$	Br	$\Gamma_{thy}$	$\Gamma_{thy}$	Br	$\Gamma_{thy}$	$\Gamma_{thy}$	Br	$\Gamma_{thy}$	$\Gamma_{thy}$	Br	$\Gamma_{thy}$	$\Gamma_{thy}$	Br	$\Gamma_{thy}$	$\Gamma_{thy}$	Br
4296	4350		4293	4351		4297	4352		4298	4348		4343	4334		4343	4348	
DD	DD	Br	DD	DD	Br	DD	DD	Br	DD	DD	Br	DD	DD	Br	DD	DD	Br
24.28	62.61%	34	22.2	35.94%	15	31.01	69.67%	27	0.21	1.26%	12	13.79%	10.12	36.17%	14.83	51.65%	12.14
11.99	30.92%	24	17.95	29.06%	2	13.1	29.43%	27	1.68	10.04%	31	35.63%	1.14	4.07%	7.93	27.62%	4.93
2.04	5.26%	11	19.9	32.22%	41	0.03	0.07%	0.6	14.24	85.12%	21	24.14%	8.88	31.74%	0.01	0.03%	0.01
0.02	0.02%	0.02	0.47	0.76%	105	0.03	0.07%	3.4	0.05	0.30%	0.5	0.57%	5.25	18.76%	1.81	6.30%	0.47
0.03	0.03%	0.03	0.38	0.62%	0.3	0.03	0.07%	0.2	0.04	0.05%	0.2	2.30%	1.97	7.04%	1.92	6.69%	2.23
0.006	0.01%	0.006	0.76	1.23%	1.1	0.03	0.07%	0.2	0.06	0.07%	0.06	0.07%	0.06	0.07%	1.61	5.61%	0.42
0.27	0.70%	12	0.76	1.23%	1.1	0.22	0.49%	13	0.05	0.30%	5	5.75%	0.32	1.15%	0.32	1.46%	0.22
0.2	0.52%	6	0.11	0.18%	2.7	0.15	0.34%	4.3	0.21	1.26%	4.3	4.94%	0.31	1.11%	0.18	0.63%	0.13
0.3	0.28%	0.3	0.11	0.18%	2.7	0.15	0.34%	4.3	0.34	2.03%	11	12.64%	0.17	0.61%	0.54	2.26%	0.54
38.78	100%	109	61.77	100%	180	44.51	100%	110	16.73	100%	87	100%	27.98	100%	28.71	100%	23.91
$3^3F_3$			$3^3F_2$			$3^3F_4$			$2^3G_4$			$2^3G_3$			$3^3G_4$		
Our	Ref. [46]		Our	Ref. [46]		Our	Ref. [46]		Our	Ref. [46]		Our	Ref. [46]		Our	Ref. [46]	
$\Gamma_{thy}$	$\Gamma_{thy}$	Br	$\Gamma_{thy}$	$\Gamma_{thy}$	Br	$\Gamma_{thy}$	$\Gamma_{thy}$	Br	$\Gamma_{thy}$	$\Gamma_{thy}$	Br	$\Gamma_{thy}$	$\Gamma_{thy}$	Br	$\Gamma_{thy}$	$\Gamma_{thy}$	Br
4457	4454		4457	4459		4454	4459		4424	4425		4424	4425		4424	4425	
DD	DD	Br	DD	DD	Br	DD	DD	Br	DD	DD	Br	DD	DD	Br	DD	DD	Br
14.98	48.64%	12.3	18.02	51.59%	18.02	21.64	53.12%	13.72	21.64	53.12%	13.72	33.68%	5.85	13.30%	10 <sup>-3</sup>	6.16%	10 <sup>-3</sup>
8.3	26.95%	13.11	8.97	25.68%	10.2	13.72	33.68%	5.85	13.72	33.68%	5.85	13.30%	5.85	13.30%	8.2	30.24%	6.53
1.57	5.10%	0.04	0.04	0.11%	0.04	1.87	4.59%	1.87	0.99	2.25%	1.61	3.77%	0.33	1.51%	0.01	0.04%	0.01
0.01	0.03%	0.01	0.01	0.03%	0.01	0.01	0.02%	0.01	0.01	0.02%	0.01	0.02%	0.01	0.02%	0.01	0.04%	0.01
0.01	0.03%	0.01	0.01	0.03%	0.01	0.01	0.02%	0.01	0.01	0.02%	0.01	0.02%	0.01	0.02%	0.01	0.04%	0.01
5.31	17.24%	1.35	6.76	19.35%	0.4	2.85	7.00%	2.85	1.65	3.75%	1.85	4.33%	0.95	2.71%	1.31	4.83%	0.98
0.01	0.03%	0.01	0.19	0.54%	0.17	10 <sup>-3</sup>	10 <sup>-3</sup>	10 <sup>-3</sup>	0.38	0.86%	0.33	0.77%	0.24	0.69%	0.01	0.04%	0.01
0.13	0.42%	0.18	0.14	0.40%	0.04	0.14	0.40%	0.04	0.01	0.02%	0.01	0.02%	0.01	0.02%	0.01	0.04%	0.01
0.14	0.45%	0.05	0.11	0.29%	0.09	0.11	0.29%	0.09	0.01	0.02%	0.01	0.02%	0.01	0.02%	0.01	0.04%	0.01
0.01	0.03%	0.01	0.01	0.03%	0.01	0.01	0.02%	0.01	0.01	0.02%	0.01	0.02%	0.01	0.02%	0.01	0.04%	0.01
0.01	0.03%	0.01	0.01	0.03%	0.01	0.01	0.02%	0.01	0.01	0.02%	0.01	0.02%	0.01	0.02%	0.01	0.04%	0.01
0.23	0.75%	0.01	0.2	0.57%	0.2	0.54	1.33%	0.54	0.85	1.93%	0.67	1.57%	0.02	0.06%	0.33	1.22%	0.4
0.11	0.36%	0.09	0.09	0.26%	0.09	0.04	0.10%	0.04	0.08	0.18%	0.05	0.12%	0.05	0.14%	0.05	0.18%	0.05
0.01	0.03%	10 <sup>-3</sup>	10 <sup>-3</sup>	10 <sup>-3</sup>	10 <sup>-3</sup>	0.06	0.15%	0.06	0.06	0.15%	0.06	0.15%	0.06	0.15%	0.06	0.15%	0.06
30.8	100.00%	43.73	34.93	100.00%	14.66	40.74	100.00%	43.98	42.76	100.00%	35	100.00%	27.12	100.00%	28.23	100.00%	23

TABLE II: The open charm decay of the  $D$ -,  $F$ -, and  $G$ -wave states is compared with the results from Ref. [46]. When the two body strong decay channels are not open or forbidden, a symbol "X" is presented. "0" denotes that the predicted values are negligibly small. All results are in units of MeV.

	$2^3D_1$	$3^3D_1$	$2^3D_2$	$3^3D_2$	$2^3D_3$	$3^3D_3$	$1^3F_3$	$2^3G_3$	$3^3G_3$	$1^3G_4$	$2^3G_4$	$3^3G_4$	$1^3G_5$	$2^3G_5$	$3^3G_5$
$1^1S_0\gamma$	0.16	0.11	0.49	0.38	0.32	0.26	8.55	7.08	4.97	$\sim 10^{-3}$	$\sim 10^{-3}$	0.01	$\sim 10^{-3}$	$\sim 10^{-3}$	0.01
$2^1S_0\gamma$	0.05	0.06	0.09	0.13	0.04	0.07	3.25	0.88	2.09	$\sim 10^{-3}$	$\sim 10^{-3}$	$\sim 10^{-4}$	$\sim 10^{-3}$	$\sim 10^{-5}$	$\sim 10^{-5}$
$3^1S_0\gamma$	$\sim 10^{-4}$	0.01	$\sim 10^{-4}$	0.02	$\sim 10^{-4}$	0.01	$\sim 10^{-5}$	1.79	0.06	$\sim 10^{-7}$	$\sim 10^{-6}$	$\sim 10^{-4}$	$\sim 10^{-6}$	$\sim 10^{-4}$	$\sim 10^{-4}$
$4^1S_0\gamma$	$\times$	$\sim 10^{-4}$	$\times$	$\sim 10^{-5}$	$\times$	$\sim 10^{-5}$	$\times$	$\sim 10^{-6}$	0.91	$\times$	$\sim 10^{-7}$	$\sim 10^{-5}$	$\times$	$\sim 10^{-7}$	$\sim 10^{-5}$
$1^3P_0\gamma$	82.20	32.32	0.93	0.65	0.29	0.33	0.17	0.15	0.11	14.82	11.26	7.40	0.03	0.04	$\sim 10^{-4}$
$2^3P_0\gamma$	126.39	43.99	0.09	0.16	0.06	0.11	$\sim 10^{-4}$	0.01	0.02	1.46	0.61	1.51	$\sim 10^{-3}$	0.01	0.01
$3^3P_0\gamma$	$\times$	119.16	$\times$	0.04	$\times$	0.07	$\times$	$\sim 10^{-5}$	$\sim 10^{-3}$	$\sim 10^{-4}$	1.35	0.01	$\sim 10^{-9}$	$\sim 10^{-4}$	0.01
$4^3P_0\gamma$	$\times$	$\times$	$\times$	$\times$	$\times$	$\times$	$\times$	$\sim 10^{-5}$	$\sim 10^{-4}$	$\times$	$\sim 10^{-4}$	0.64	$\times$	$\sim 10^{-10}$	$\sim 10^{-4}$
$1^3P_1\gamma$	26.35	7.84	49.12	17.88	1.24	0.96	0.34	0.29	0.21	14.15	9.49	5.75	15.80	0.07	0.02
$2^3P_1\gamma$	115.98	25.57	127.69	38.40	0.22	0.62	$\sim 10^{-4}$	0.05	0.08	1.71	1.66	2.75	2.11	1.71	0.03
$3^3P_1\gamma$	$\times$	90.29	$\times$	81.40	$\times$	0.11	$\times$	$\sim 10^{-4}$	0.01	$\sim 10^{-4}$	1.12	0.12	$\sim 10^{-5}$	1.42	$\sim 10^{-3}$
$4^3P_1\gamma$	$\times$	$\times$	$\times$	$\times$	$\times$	$\times$	$\times$	$\sim 10^{-5}$	$\times$	$\sim 10^{-5}$	$\times$	0.55	$\times$	$\sim 10^{-10}$	$\sim 10^{-4}$
$1^3P_2\gamma$	5.43	2.50	10.90	3.55	40.99	13.06	0.42	0.28	0.17	2.86	1.63	0.91	10.19	6.23	7.99
$2^3P_2\gamma$	11.86	6.95	63.34	12.27	212.66	47.21	$\sim 10^{-3}$	0.13	0.14	0.43	0.75	0.85	1.70	2.26	6.24
$3^3P_2\gamma$	$\times$	6.37	$\times$	26.13	$\times$	93.97	$\times$	$\sim 10^{-5}$	$\times$	$\sim 10^{-7}$	0.16	0.08	$\sim 10^{-6}$	0.64	1.57
$4^3P_2\gamma$	$\times$	$\times$	$\times$	$\times$	$\times$	$\times$	$\times$	$\sim 10^{-5}$	$\times$	$\sim 10^{-7}$	$\times$	0.08	$\times$	$\sim 10^{-6}$	0.80
$1^1D_2\gamma$	0.04	0.04	0.04	0.02	0.15	0.12	249.14	42.32	13.89	0.13	0.09	0.05	0.24	0.19	0.08
$2^1D_2\gamma$	0.02	0.02	$\times$	0.02	$\sim 10^{-5}$	0.07	$\times$	154.09	40.82	$\sim 10^{-4}$	0.03	0.03	$\sim 10^{-4}$	0.05	0.04
$3^1D_2\gamma$	$\times$	0.03	$\times$	$\times$	$\times$	$\sim 10^{-4}$	$\times$	$\times$	94.51	$\times$	$\sim 10^{-5}$	0.01	$\times$	$\sim 10^{-5}$	0.01
$4^1D_2\gamma$	$\times$	$\times$	$\times$	$\times$	$\times$	$\times$	$\times$	$\times$	$\times$	$\times$	$\times$	$\sim 10^{-5}$	$\times$	$\times$	$\sim 10^{-5}$
$1^3F_2\gamma$	17.19	0.15	0.72	0.11	0.02	0.02	$\sim 10^{-5}$	0.03	0.03	219.87	38.11	12.52	0.20	0.30	0.01
$2^3F_2\gamma$	$\times$	32.17	$\times$	0.86	$\times$	0.02	$\times$	$\sim 10^{-5}$	0.02	$\times$	129.88	36.55	$\times$	0.08	$\sim 10^{-3}$
$3^3F_2\gamma$	$\times$	$\times$	$\times$	$\times$	$\times$	$\times$	$\times$	$\times$	$\sim 10^{-5}$	$\times$	$\times$	76.66	$\times$	$\times$	$\sim 10^{-3}$
$1^3F_3\gamma$	$\sim 10^{-3}$	0.37	5.37	0.03	0.56	0.10	$\times$	0.02	0.01	21.54	3.63	1.23	204.82	31.90	0.16
$2^3F_3\gamma$	$\times$	0.01	$\times$	6.13	$\times$	0.65	$\times$	$\times$	0.01	$\times$	12.41	3.43	$\times$	124.34	0.12
$3^3F_3\gamma$	$\times$	$\times$	$\times$	$\times$	$\times$	$\times$	$\times$	$\times$	$\times$	$\times$	$\times$	7.19	$\times$	$\times$	0.02
$1^3F_4\gamma$	$\sim 10^{-5}$	0.06	$\sim 10^{-3}$	0.14	7.30	0.21	$\times$	$\sim 10^{-3}$	$\sim 10^{-3}$	0.41	0.11	0.05	15.73	2.83	8.48
$2^3F_4\gamma$	$\times$	$\sim 10^{-4}$	$\times$	$\sim 10^{-4}$	$\times$	8.07	$\times$	$\times$	$\sim 10^{-3}$	$\times$	$\times$	9.15	$\times$	9.15	126.53
$3^3F_4\gamma$	$\times$	$\times$	$\times$	$\times$	$\times$	$\times$	$\times$	$\times$	$\times$	$\times$	$\times$	5.12	$\times$	$\times$	73.64
$1^1G_4\gamma$	$\times$	$\times$	$\times$	$\sim 10^{-5}$	$\times$	$\sim 10^{-5}$	$\times$	3.19	0.11	$\sim 10^{-5}$	$\sim 10^{-3}$	$\sim 10^{-3}$	$\sim 10^{-3}$	0.01	0.01
$2^1G_4\gamma$	$\times$	$\times$	$\times$	$\times$	$\times$	$\times$	$\times$	$\times$	3.30	$\times$	$\sim 10^{-6}$	$\sim 10^{-3}$	$\times$	$\times$	$\sim 10^{-3}$

TABLE III: Radiative decay behavior of these discussed high-lying charmonia. The symbol " $\times$ " indicates that the radiative decay channels are forbidden. All results are in units of keV.



	$2^1D_2$	$3^1D_2$	$1^3F_2$	$2^3F_2$	$3^3F_2$	$1^3F_3$	$2^3F_3$	$3^3F_3$	$1^3F_4$	$2^3F_4$	$3^3F_4$	$1^1G_4$	$2^1G_4$	$3^1G_4$
$1^3S_1\gamma$	0.64	0.44	11.36	7.62	4.66	9.99	7.17	4.57	8.13	6.05	3.97	0.01	0.02	0.01
$2^3S_1\gamma$	0.15	0.20	1.85	2.43	3.49	1.95	1.75	2.81	1.87	1.20	2.12	$\sim 10^{-3}$	$\sim 10^{-6}$	$\sim 10^{-3}$
$3^3S_1\gamma$	$\sim 10^{-3}$	0.04	$\sim 10^{-7}$	1.19	0.47	$\sim 10^{-7}$	1.25	0.28	$\sim 10^{-6}$	1.19	0.17	$\sim 10^{-6}$	$\sim 10^{-3}$	$\sim 10^{-4}$
$4^3S_1\gamma$	$\times$	$\sim 10^{-3}$	$\times$	$\sim 10^{-4}$	3.61	$\times$	$\sim 10^{-3}$	3.65	$\times$	$\sim 10^{-3}$	3.56	$\times$	$\sim 10^{-5}$	$\sim 10^{-3}$
$1^1P_1\gamma$	58.45	21.04	0.19	0.13	0.08	0.42	0.33	0.23	0.25	0.22	0.16	24.29	16.49	10.03
$2^1P_1\gamma$	167.10	49.09	$\sim 10^{-4}$	0.04	0.04	$\sim 10^{-4}$	0.07	0.10	$\sim 10^{-4}$	0.04	0.06	3.09	3.07	4.92
$3^1P_1\gamma$	$\times$	105.64	$\times$	$\sim 10^{-4}$	0.01	$\times$	$\sim 10^{-4}$	0.02	$\times$	$\sim 10^{-5}$	0.01	$\sim 10^{-5}$	2.10	0.25
$4^1P_1\gamma$	$\times$	$\times$	$\times$	$\times$	$\sim 10^{-5}$	$\times$	$\times$	$\sim 10^{-5}$	$\times$	$\times$	$\sim 10^{-5}$	$\times$	$\sim 10^{-5}$	1.04
$1^3D_1\gamma$	0.28	0.17	439.69	73.05	24.00	1.12	1.22	0.83	0.02	0.07	0.05	0.21	0.16	0.10
$2^3D_1\gamma$	$\times$	0.03	$\times$	76.97	29.52	$\times$	0.05	0.19	$\times$	$\sim 10^{-3}$	0.01	$\sim 10^{-5}$	0.01	0.02
$3^3D_1\gamma$	$\times$	$\times$	$\times$	$\times$	30.37	$\times$	$\times$	0.01	$\times$	$\times$	$\sim 10^{-4}$	$\times$	$\sim 10^{-6}$	$\sim 10^{-3}$
$4^3D_1\gamma$	$\times$	$\times$	$\times$	$\times$	$\times$	$\times$	$\times$	$\times$	$\times$	$\times$	$\times$	$\times$	$\times$	$\sim 10^{-5}$
$1^3D_2\gamma$	0.10	0.06	60.89	9.37	3.05	295.43	45.97	14.29	0.41	0.69	0.48	0.27	0.20	0.13
$2^3D_2\gamma$	$\times$	0.03	$\times$	27.01	7.11	$\times$	137.72	36.31	$\times$	0.11	0.30	$\sim 10^{-4}$	0.04	0.05
$3^3D_2\gamma$	$\times$	$\times$	$\times$	$\times$	15.86	$\times$	$\times$	82.87	$\times$	$\times$	0.05	$\times$	$\sim 10^{-5}$	0.01
$4^3D_2\gamma$	$\times$	$\times$	$\times$	$\times$	$\times$	$\times$	$\times$	$\times$	$\times$	$\times$	$\times$	$\times$	$\times$	$\sim 10^{-5}$
$1^3D_3\gamma$	0.01	0.01	1.79	0.54	0.25	38.83	5.95	1.92	269.26	38.03	11.37	0.27	0.18	0.11
$2^3D_3\gamma$	$\times$	$\sim 10^{-4}$	$\times$	0.85	0.36	$\times$	19.16	4.81	$\times$	141.37	33.97	$\sim 10^{-4}$	0.05	0.06
$3^3D_3\gamma$	$\times$	$\times$	$\times$	$\times$	0.49	$\times$	$\times$	11.28	$\times$	$\times$	89.20	$\times$	$\sim 10^{-5}$	0.01
$4^3D_3\gamma$	$\times$	$\times$	$\times$	$\times$	$\times$	$\times$	$\times$	$\times$	$\times$	$\times$	$\times$	$\times$	$\times$	$\sim 10^{-5}$
$1^1F_3\gamma$	6.28	0.26	$\times$	$\sim 10^{-3}$	$\sim 10^{-3}$	$\sim 10^{-6}$	0.02	0.01	$\sim 10^{-5}$	0.04	0.03	214.94	34.28	10.74
$2^1F_3\gamma$	$\times$	7.29	$\times$	$\times$	$\times$	$\times$	$\times$	0.01	$\times$	$\sim 10^{-5}$	0.02	$\times$	133.06	34.10
$3^1F_3\gamma$	$\times$	$\times$	$\times$	$\times$	$\times$	$\times$	$\times$	$\times$	$\times$	$\sim 10^{-3}$	$\times$	$\times$	$\times$	77.78
$1^3G_3\gamma$	$\times$	$\sim 10^{-5}$	$\times$	2.29	0.06	$\times$	0.14	0.03	$\times$	$\sim 10^{-3}$	$\times$	$\times$	0.01	0.01
$2^3G_3\gamma$	$\times$	$\times$	$\times$	$\times$	2.51	$\times$	$\times$	0.16	$\times$	$\times$	$\times$	$\times$	$\times$	$\sim 10^{-3}$
$1^3G_4\gamma$	$\times$	$\sim 10^{-5}$	$\times$	$\sim 10^{-4}$	0.04	$\times$	2.82	0.04	$\times$	0.14	0.02	$\times$	0.01	0.01
$2^3G_4\gamma$	$\times$	$\times$	$\times$	$\times$	$\sim 10^{-5}$	$\times$	$\times$	2.84	$\times$	$\times$	0.16	$\times$	$\times$	$\sim 10^{-3}$
$1^3G_5\gamma$	$\times$	$\sim 10^{-5}$	$\times$	$\sim 10^{-7}$	$\sim 10^{-3}$	$\times$	$\sim 10^{-4}$	0.03	$\times$	3.65	0.11	$\sim 10^{-6}$	$\sim 10^{-3}$	$\sim 10^{-3}$
$2^3G_5\gamma$	$\times$	$\times$	$\times$	$\times$	$\sim 10^{-7}$	$\times$	$\times$	$\sim 10^{-4}$	$\times$	$\times$	3.25	$\times$	$\times$	$\sim 10^{-3}$

TABLE IV: Radiative decay behavior of these discussed high-lying charmonia. All results are in units of keV.

- and T.-M. Yan, The spectrum of charmonium, *Phys. Rev. Lett.* **34**, 369 (1975), [Erratum: *Phys.Rev.Lett.* 36, 1276 (1976)].
- [14] E. Eichten, K. Gottfried, T. Kinoshita, K. D. Lane, and T.-M. Yan, Charmonium: the model, *Phys. Rev. D* **17**, 3090 (1978), [Erratum: *Phys.Rev.D* 21, 313 (1980)].
- [15] R. Barbieri, R. Kogerler, Z. Kunszt, and R. Gatto, Meson masses and widths in a Gauge theory with linear binding potential, *Nucl. Phys. B* **105**, 125 (1976).
- [16] D. P. Stanley and D. Robson, Nonperturbative potential model for light and heavy quark anti-quark systems, *Phys. Rev. D* **21**, 3180 (1980).
- [17] J. Carlson, J. B. Kogut, and V. R. Pandharipande, Hadron spectroscopy in a flux tube quark model, *Phys. Rev. D* **28**, 2807 (1983).
- [18] J. L. Richardson, The heavy quark potential and the  $\Upsilon$ ,  $J/\psi$  Systems, *Phys. Lett. B* **82**, 272 (1979).
- [19] W. Buchmuller, G. Grunberg, and S. H. H. Tye, The Regge slope and the Lambda parameter in QCD: An empirical approach via quarkonia, *Phys. Rev. Lett.* **45**, 103 (1980), [Erratum: *Phys.Rev.Lett.* 45, 587 (1980)].
- [20] W. Buchmuller and S. H. H. Tye, Quarkonia and quantum chromodynamics, *Phys. Rev. D* **24**, 132 (1981).
- [21] A. Martin, A simultaneous fit of  $b\bar{b}$ ,  $c\bar{c}$ ,  $s\bar{s}$ , ( $bcs$  pairs) and  $c\bar{s}$  Spectra, *Phys. Lett. B* **100**, 511 (1981).
- [22] G. Bhanot and S. Rudaz, A New Potential for Quarkonium, *Phys. Lett. B* **78**, 119 (1978).
- [23] C. Quigg and J. L. Rosner, Quarkonium Level Spacings, *Phys. Lett. B* **71**, 153 (1977).
- [24] S. Godfrey and N. Isgur, Mesons in a relativized quark model with chromodynamics, *Phys. Rev. D* **32**, 189 (1985).
- [25] L. P. Fulcher, Perturbative QCD, a universal QCD scale, long range spin orbit potential, and the properties of heavy quarkonia, *Phys. Rev. D* **44**, 2079 (1991).
- [26] S. N. Gupta, J. M. Johnson, W. W. Repko, and C. J. Suchyta, III, Heavy quarkonium potential model and the P-wave singlet state of charmonium, *Phys. Rev. D* **49**, 1551 (1994).

- [27] J. Zeng, J. W. Van Orden, and W. Roberts, Heavy mesons in a relativistic model, *Phys. Rev. D* **52**, 5229 (1995).
- [28] D. Ebert, R. N. Faustov, and V. O. Galkin, Properties of heavy quarkonia and  $B_c$  mesons in the relativistic quark model, *Phys. Rev. D* **67**, 014027 (2003).
- [29] X. Liu, Z.-G. Luo, Y.-R. Liu, and S.-L. Zhu, X(3872) and other possible heavy molecular states, *Eur. Phys. J. C* **61**, 411 (2009).
- [30] X. Liu, An overview of XYZ new particles, *Chin. Sci. Bull.* **59**, 3815 (2014).
- [31] H.-X. Chen, W. Chen, X. Liu, and S.-L. Zhu, The hidden-charm pentaquark and tetraquark states, *Phys. Rept.* **639**, 1 (2016).
- [32] F.-K. Guo, C. Hanhart, U.-G. Meißner, Q. Wang, Q. Zhao, and B.-S. Zou, Hadronic molecules, *Rev. Mod. Phys.* **90**, 015004 (2018), [Erratum: *Rev. Mod. Phys.* **94**, 029901 (2022)], [arXiv:1705.00141 \[hep-ph\]](#).
- [33] N. Brambilla, S. Eidelman, C. Hanhart, A. Nefediev, C.-P. Shen, C. E. Thomas, A. Vairo, and C.-Z. Yuan, The XYZ states: experimental and theoretical status and perspectives, *Phys. Rept.* **873**, 1 (2020), [arXiv:1907.07583 \[hep-ex\]](#).
- [34] H.-X. Chen, W. Chen, X. Liu, Y.-R. Liu, and S.-L. Zhu, An updated review of the new hadron states, *Rept. Prog. Phys.* **86**, 026201 (2023).
- [35] Q. Deng, R.-H. Ni, Q. Li, and X.-H. Zhong, Charmonia in an unquenched quark model, *Phys. Rev. D* **110**, 056034 (2024).
- [36] S. K. Choi *et al.* (Belle), Observation of a narrow charmonium-like state in exclusive  $B^+ \rightarrow K^+ \pi^+ \pi^- J/\psi$  decays, *Phys. Rev. Lett.* **91**, 262001 (2003).
- [37] C.-Y. Wong, Molecular states of heavy quark mesons, *Phys. Rev. C* **69**, 055202 (2004).
- [38] E. S. Swanson, Short range structure in the X(3872), *Phys. Lett. B* **588**, 189 (2004).
- [39] L. Maiani, F. Piccinini, A. D. Polosa, and V. Riquer, Diquark-antidiquarks with hidden or open charm and the nature of X(3872), *Phys. Rev. D* **71**, 014028 (2005).
- [40] W. Chen and S.-L. Zhu, The vector and axial-vector charmonium-like states, *Phys. Rev. D* **83**, 034010 (2011).
- [41] E. van Beveren and G. Rupp, Observed  $D_s(2317)$  and tentative  $D(2100-2300)$  as the charmed cousins of the light scalar nonet, *Phys. Rev. Lett.* **91**, 012003 (2003).
- [42] Y.-B. Dai, C.-S. Huang, C. Liu, and S.-L. Zhu, Understanding the  $D_{sJ}^+(2317)$  and  $D_{sJ}^+(2460)$  with sum rules in HQET, *Phys. Rev. D* **68**, 114011 (2003).
- [43] E. van Beveren and G. Rupp, Continuum bound states  $K_L$ ,  $D_1(2420)$ ,  $D_{s1}(2536)$  and their partners  $K_S$ ,  $D_1(2400)$ ,  $D_{sJ}^*(2463)$ , *Eur. Phys. J. C* **32**, 493 (2004).
- [44] Y. S. Kalashnikova, Coupled-channel model for charmonium levels and an option for X(3872), *Phys. Rev. D* **72**, 034010 (2005).
- [45] O. Zhang, C. Meng, and H. Q. Zheng, Ambivalence of X(3872), *Phys. Lett. B* **680**, 453 (2009).
- [46] T. Barnes, S. Godfrey, and E. S. Swanson, Higher charmonia, *Phys. Rev. D* **72**, 054026 (2005).
- [47] M.-X. Duan, S.-Q. Luo, X. Liu, and T. Matsuki, Possibility of charmoniumlike state X(3915) as  $\chi_{c0}(2P)$  state, *Phys. Rev. D* **101**, 054029 (2020).
- [48] Z.-L. Man, C.-R. Shu, Y.-R. Liu, and H. Chen, Charmonium states in a coupled-channel model, *Eur. Phys. J. C* **84**, 810 (2024).
- [49] R. Aaij *et al.* (LHCb), Near-threshold  $D\bar{D}$  spectroscopy and observation of a new charmonium state, *JHEP* **07**, 035.
- [50] R. Aaij *et al.* (LHCb), Observation of new charmonium or charmoniumlike states in  $B^+ \rightarrow D^{*+} D^+ K^+$  Decays, *Phys. Rev. Lett.* **133**, 131902 (2024).
- [51] M. Ablikim *et al.* (BESIII), Observation of Structures in the Processes  $e^+e^- \rightarrow \omega\chi_{c1}$  and  $\omega\chi_{c2}$ , *Phys. Rev. Lett.* **132**, 161901 (2024).
- [52] M. Ablikim *et al.* (BESIII), Observation of a vector charmoniumlike state at 4.7 GeV/c<sup>2</sup> and Search for  $Z_{cs}$  in  $e^+e^- \rightarrow K^+K^-J/\psi$ , *Phys. Rev. Lett.* **131**, 211902 (2023).
- [53] M. Ablikim *et al.* (BESIII), Precise Measurement of the  $e^+e^- \rightarrow D_s^{*+}D_s^{*-}$  Cross Sections at Center-of-Mass Energies from Threshold to 4.95 GeV, *Phys. Rev. Lett.* **131**, 151903 (2023).
- [54] S. Navas *et al.* (Particle Data Group), Review of particle physics, *Phys. Rev. D* **110**, 030001 (2024).
- [55] H.-X. Chen, W. Chen, X. Liu, Y.-R. Liu, and S.-L. Zhu, A review of the open charm and open bottom systems, *Rept. Prog. Phys.* **80**, 076201 (2017), [arXiv:1609.08928 \[hep-ph\]](#).
- [56] J.-Z. Wang, D.-Y. Chen, X. Liu, and T. Matsuki, Constructing  $J/\psi$  family with updated data of charmoniumlike Y states, *Phys. Rev. D* **99**, 114003 (2019).
- [57] M.-X. Duan and X. Liu, Where are 3P and higher P-wave states in the charmonium family?, *Phys. Rev. D* **104**, 074010 (2021).
- [58] C. A. Bokade and Bhaghyesh, Charmonium: conventional and XYZ states in a relativistic screened potential model, [arXiv:2408.06759 \[hep-ph\]](#).
- [59] W.-J. Deng, H. Liu, L.-C. Gui, and X.-H. Zhong, Charmonium spectrum and their electromagnetic transitions with higher multipole contributions, *Phys. Rev. D* **95**, 034026 (2017).
- [60] B.-Q. Li and K.-T. Chao, Higher charmonia and X,Y,Z states with screened potential, *Phys. Rev. D* **79**, 094004 (2009).
- [61] R. Chaturvedi and A. K. Rai, Charmonium spectroscopy motivated by general features of pNRQCD, *Int. J. Theor. Phys.* **59**, 3508 (2020).
- [62] M. A. Sultan, N. Akbar, B. Masud, and F. Akram, Higher hybrid charmonia in an extended potential model, *Phys. Rev. D* **90**, 054001 (2014).
- [63] R. N. Faustov, D. Ebert, and V. O. Galkin, Spectroscopy and Regge trajectories of heavy quarkonia and  $B_c$  mesons, *PoS Baldin-ISHEPP-XXI*, 058 (2012).
- [64] L. Cao, Y.-C. Yang, and H. Chen, Charmonium states in QCD-inspired quark potential model using Gaussian expansion method, *Few Body Syst.* **53**, 327 (2012).
- [65] Q.-T. Song, D.-Y. Chen, X. Liu, and T. Matsuki, Charmed-strange mesons revisited: mass spectra and strong decays, *Phys. Rev. D* **91**, 054031 (2015).
- [66] Q.-T. Song, D.-Y. Chen, X. Liu, and T. Matsuki, Higher radial and orbital excitations in the charmed meson family, *Phys. Rev. D* **92**, 074011 (2015).
- [67] C.-Q. Pang, J.-Z. Wang, X. Liu, and T. Matsuki, A systematic study of mass spectra and strong decay of strange mesons, *Eur. Phys. J. C* **77**, 861 (2017).
- [68] J.-Z. Wang, Z.-F. Sun, X. Liu, and T. Matsuki, Higher bottomonium zoo, *Eur. Phys. J. C* **78**, 915 (2018).
- [69] J.-Z. Wang, R.-Q. Qian, X. Liu, and T. Matsuki, Are the Y states around 4.6 GeV from  $e^+e^-$  annihilation higher charmonia?, *Phys. Rev. D* **101**, 034001 (2020).
- [70] L.-M. Wang, S.-Q. Luo, and X. Liu, Light unflavored vector meson spectroscopy around the mass range of 2.4-3 GeV and possible experimental evidence, *Phys. Rev. D* **105**, 034011 (2022).
- [71] L. Micu, Decay rates of meson resonances in a quark model, *Nucl. Phys. B* **10**, 521 (1969).
- [72] A. Le Yaouanc, L. Oliver, O. Pene, and J. C. Raynal, Naive quark pair creation model and baryon decays, *Phys. Rev. D* **9**, 1415 (1974).
- [73] A. Le Yaouanc, L. Oliver, O. Pene, and J. C. Raynal, Why is  $\psi''(4.414)$  so narrow?, *Phys. Lett. B* **72**, 57 (1977).

- [74] A. Le Yaouanc, L. Oliver, O. Pene, and J. C. Raynal, Strong decays of  $\psi''(4.028)$  as a radial excitation of charmonium, *Phys. Lett. B* **71**, 397 (1977).
- [75] Y.-B. Ding, K.-T. Chao, and D.-H. Qin, Possible effects of color screening and large string tension in heavy quarkonium spectra, *Phys. Rev. D* **51**, 5064 (1995).
- [76] K. D. Born, E. Laermann, N. Pirch, T. F. Walsh, and P. M. Zerwas, Hadron Properties in Lattice QCD With Dynamical Fermions, *Phys. Rev. D* **40**, 1653 (1989).
- [77] Z.-Y. Bai, Q.-S. Zhou, and X. Liu, Role of  $4S$ - $3D$  mixing in explaining the  $\omega$ -like  $Y(2119)$  observed in  $e^+e^- \rightarrow \rho\pi$  and  $\rho(1450)\pi$ , *Phys. Rev. D* **111**, 054013 (2025), [arXiv:2502.05754 \[hep-ph\]](#).
- [78] B.-Q. Li, C. Meng, and K.-T. Chao, Coupled-Channel and Screening Effects in Charmonium Spectrum, *Phys. Rev. D* **80**, 014012 (2009), [arXiv:0904.4068 \[hep-ph\]](#).
- [79] L. Liu, G. Moir, M. Peardon, S. M. Ryan, C. E. Thomas, P. Vilaseca, J. J. Dudek, R. G. Edwards, B. Joo, and D. G. Richards (Hadron Spectrum), Excited and exotic charmonium spectroscopy from lattice QCD, *JHEP* **07**, 126.
- [80] T.-C. Peng, Z.-Y. Bai, J.-Z. Wang, and X. Liu, Reevaluating the  $\psi(4160)$  resonance parameter using  $B^+ \rightarrow K^+\mu^+\mu^-$  data in the context of unquenched charmonium spectroscopy, *Phys. Rev. D* **111**, 054023 (2025).
- [81] M. Jacob and G. C. Wick, On the general theory of collisions for particles with spin, *Annals Phys.* **7**, 404 (1959).
- [82] S. J. Brodsky and J. R. Primack, The electromagnetic interactions of composite systems, *Annals Phys.* **52**, 315 (1969).
- [83] F. E. Close and L. A. Copley, Electromagnetic interactions of weakly bound composite systems, *Nucl. Phys. B* **19**, 477 (1970).
- [84] Z.-P. Li, The threshold pion photoproduction of nucleons in the chiral quark model, *Phys. Rev. D* **50**, 5639 (1994).
- [85] Z.-p. Li, H.-x. Ye, and M.-h. Lu, An unified approach to pseudoscalar meson photoproductions off nucleons in the quark model, *Phys. Rev. C* **56**, 1099 (1997).
- [86] K.-L. Wang, Y.-X. Yao, X.-H. Zhong, and Q. Zhao, Strong and radiative decays of the low-lying S- and P-wave singly heavy baryons, *Phys. Rev. D* **96**, 116016 (2017).
- [87] V. Bhardwaj *et al.* (Belle), Evidence of a new narrow resonance decaying to  $\chi_{c1}\gamma$  in  $B \rightarrow \chi_{c1}\gamma K$ , *Phys. Rev. Lett.* **111**, 032001 (2013), [arXiv:1304.3975 \[hep-ex\]](#).
- [88] R. Aaij *et al.* (LHCb), Study of the  $\psi_2(3823)$  and  $\chi_{c1}(3872)$  states in  $B^+ \rightarrow (J\psi\pi^+\pi^-)K^+$  decays, *JHEP* **08**, 123, [arXiv:2005.13422 \[hep-ex\]](#).